2

Technical Document 2226
October 1991

Beamforming With a Limited Number of Snapshots

C. V. Tran

Approved for public release; distribution is unlimited.

ADMINISTRATIVE INFORMATION

The work in this report was carried out by the Processing Research and Development Branch (Code 761) of the Naval Ocean Systems Center, San Diego, CA. Sponsorship was provided by Office of Chief of Naval Research, Arlington, VA.

Released by
G. W. Byram, Head
Processing Research
and Development Branch

Under authority of
J. Wangler, Acting Head
Space Systems and
Technology Division

CONTENTS

FIGURES

TABLES

1.0 INTRODUCTION

The interaction between the number of snapshots (temporal samples) and the number of sensors in adaptive beamforming is recognized in literature. It is well known from the seminal paper of Reed, Mallett, and Brennan (1974) that, compared to the ideal case of an infinite number of snapshots, the loss in signal-to-interference-plus-noise ratio of the Minimum Variance Distortionless Response (MVDR) is less than 3 dB if the number of snapshots of data is at least twice the number of array elements. More fundamentally, when the number of snapshots is fewer than the number of sensors, the sample cross-spectral density matrix $\widehat{\mathbf{R}}$ (which is also the maximum likelihood estimator of the true, but unknown, cross-spectral density matrix $\mathbf{R}$) is singular, rendering the MVDR method useless. This led Capon (1969) to modify the cross-spectral density matrix $\widehat{\mathbf{R}}$ by adding a small amount of incoherent noise to the diagonal of $\widehat{\mathbf{R}}$; the procedure now is known as diagonal loading or white-noise stabilization (Carlson, 1988; Tran, 1990).

For a very large array of size n and a relatively small number of snapshots T, the modified MVDR method encounters another problem, namely the computational load in inverting the $(n \times n)$ modified cross-spectral density matrix. The recently introduced JASON algorithm (Rothaus, 1991) requires the inversion of a $(T \times T)$ matrix, a desirable advantage especially when $T \ll n$.

The purpose of this report is to investigate properties and performance of conventional (or Bartlett), MVDR (with diagonal loading), and JASON beamformers when the number of snapshots is small compared to the number of array elements.

The remainder of the report is organized into five sections. In section 2.0, a narrowband, multiple-source model is presented. The formulation is an extension of a narrowband, single-source model presented in Rothaus (1991). This section provides notations and terminology for section 3.0 where a quick review of the three beamforming methods, conventional, MVDR, and JASON beamformers, is given with attention to the situation where the number of snapshots is small relative to the number of array elements. In section 4.0, the general model in section 2.0 is refined for simulation.

In particular, we consider an environment consisting of twenty narrowband, plane-wave sources, corrupted in additive colored noise, impinging on a uniform line array of 100 elements with interelement spacing equal to one half of the array wavelength. The noise is zero mean and may be temporally correlated from sample to sample. In section 5.0, comparative simulation results of the three beamforming methods are presented as a function of the number of snapshots that is less than or equal to the number of sensors. Qualitative results based on output array response, and quantitative results based on normalized output deflection and peak-to-background ratio, are presented in subsections 5.1 and 5 2, respectively. Finally, in section 6.0, we conclude the report by sumarizing our findings with emphasis on a well-populated array and a small number of snapshots.

An interactive code, written in MATLAB, for plotting array response is included in Appendix A.

2.0 GENERAL MODEL

In this section a general model is formulated for a narrowband, multisource environment after Rothaus (1991) where a single source is explicitly considered. Most notations and terminology in Rothaus (1991) are followed for quick reference.

Suppose we have an acoustic field of n sensors distributed in space, a point source in the direction of the steering vector α and k other sources, called interferences, with direction specified by steering vectors β_j, $j = 1, \cdots, k$.

At time t and sensor i, by changing the local time at each sensor, the observed data can be written as

$$X_i(t) \;=\; N_i(t) + \alpha_i P(t) + \sum_{j=1}^{k} \beta_{j,i} Q_j(t), \qquad (1)$$

where $N_i(t)$ denotes the noise field, $P(t)$ and $Q_j(t)$, $j = 1, \cdots, k$, are acoustic pressures, or complex magnitudes (envelopes), of sources.

By stacking expression(1) vertically, serially in i, for $i = 1, 2, \ldots, n$, we arrive at the following compact matrix notation

$$\mathbf{X}(t) \;=\; \mathbf{N}(t) \;+\; P(t)\alpha \;+\; \sum_{j=1}^{k} Q_j(t)\beta_j. \tag{2}$$

The vector $\mathbf{X}(t)$ is often referred to as the snapshot at time t.

Consider T consecutive snapshots $\mathbf{X}(t)$, $\mathbf{X}(t+1)$, $\ldots$, $\mathbf{X}(t+T-1)$. Assume that the steering vectors α, β_j, $j = 1, \ldots, k$, remain constant during the processing interval represented by the duration of the T snapshots. Let

$$\mathcal{S}(t) \triangleq \left[\mathbf{X}(t) \,\vdots\, \mathbf{X}(t+1) \,\vdots\, \cdots \,\vdots\, \mathbf{X}(t+T-1)\right],$$

$$\mathcal{N}(t) \triangleq \left[\mathbf{N}(t) \,\vdots\, \mathbf{N}(t+1) \,\cdots\, \vdots\, \mathbf{N}(t+T-1)\right],$$

and

$$\mathcal{P}(t) \triangleq \begin{bmatrix} \overline{P}(t) \\ \overline{P}(t+1) \\ \vdots \\ \overline{P}(t+T-1) \end{bmatrix}, \qquad \mathcal{Q}_j(t) \triangleq \begin{bmatrix} \overline{Q_j}(t) \\ \overline{Q_j}(t+1) \\ \vdots \\ \overline{Q_j}(t+T-1) \end{bmatrix}, \quad j = 1, 2, \cdots, k.$$

Then, we obtain

$$\mathcal{S}(t) \;=\; \mathcal{N}(t) \;+\; \alpha\mathcal{P}^*(t) \;+\; \sum_{j=1}^{k} \beta_j \mathcal{Q}_j^*(t). \tag{3}$$

Here, the "overbar" denotes complex conjugate, and *, conjugate transpose.

It follows immediately that $\widehat{\mathbf{R}}$, the maximum-likelihood estimate of the true (but unknown) cross-spectral density matrix $\mathbf{R}$ of the received pressure field can be written as

$$\widehat{\mathbf{R}} \triangleq \frac{1}{T}\sum_{\tau=t}^{t+T-1} \mathbf{X}(\tau)\mathbf{X}^*(\tau) \;=\; \frac{1}{T}\mathcal{S}(t)\mathcal{S}^*(t). \tag{4}$$

Notice that the average signal power is $\frac{1}{T}\mathcal{P}^*(t)\mathcal{P}(t)$ and, similarly, the average power of the j-th interference is $\frac{1}{T}\mathcal{Q}_j^*(t)\mathcal{Q}_j(t)$. Also, the average noise power per sensor is

$$\frac{1}{n}\,\mathrm{tr}\left(\frac{1}{T}\mathcal{N}(t)\mathcal{N}^*(t)\right) \;=\; \frac{1}{nT}\,\mathrm{tr}\left(\mathcal{N}(t)\mathcal{N}^*(t)\right),$$

where $\mathrm{tr}(\mathbf{Y})$ is the trace of matrix $\mathbf{Y}$.

The space spanned by columns of $\mathcal{S}$, which are the T snapshots, is called the observation space. These snapshots can be assumed to be linearly independent.

3.0 BEAMFORMING

A quick review of three beamforming methods, conventional, MVDR, and the recently introduced JASON, is presented in this section. Our emphasis is on the situation where the number of snapshots is relatively small compared to the number of sensors.

The MVDR beamformer is an adaptive, high-resolution beamformer that minimizes the output power while maintaining unity response in the direction of look. Mathematically, a weight vector $\mathbf{w}$ is sought after for the constrained optimization problem

$$\min_{\mathbf{w}} \mathbf{w}^*\mathbf{R}\mathbf{w} \qquad \text{subject to} \quad \mathbf{w}^*\gamma = 1, \tag{5}$$

where γ denotes the look-direction steering vector.

The optimal weight vector is readily obtained as

$$\mathbf{w} = \frac{\mathbf{R}^{-1}\gamma}{\gamma^*\mathbf{R}^{-1}\gamma},$$

which yields the optimal output power

$$\mathbf{w}^*\mathbf{R}\mathbf{w} = \frac{1}{\gamma^*\mathbf{R}^{-1}\gamma}.$$

The conventional beamformer, described by the delay-and-sum process, is equivalent to setting the weight vector equal to the look-direction steering vector γ. Its output power is $\gamma^*\mathbf{R}\gamma$.

Operationally, due to the unknown nature of the cross-spectral density matrix $\mathbf{R}$, we deal exclusively with its maximum-likelihood estimator $\widehat{\mathbf{R}}$. Thus, by replacing $\mathbf{R}$ by $\widehat{\mathbf{R}}$ and using equation (4), an operational form for problem (5) is

$$\min_{\mathbf{w}} \mathbf{w}^*\mathcal{S}\mathcal{S}^*\mathbf{w} \qquad \text{subject to} \quad \mathbf{w}^*\gamma = 1. \tag{6}$$

Here, the constant term $\frac{1}{T}$ is ignored since it has no effect on the minimization.

By taking expectation, we obtain the "true" output powers corresponding to T snapshots:

$$\text{POWER}_{\text{MVDR}} = \text{E}\left(\frac{1}{\gamma^*\widehat{\mathbf{R}}^{-1}\gamma}\right) = \frac{1}{T}\,\text{E}\left(\frac{1}{\gamma^*(\mathcal{S}\mathcal{S}^*)^{-1}\gamma}\right), \tag{7}$$

and

$$\text{POWER}_{\text{Con}} = \mathrm{E}\left(\gamma^{*}\widehat{\mathbf{R}}\gamma\right) = \frac{1}{T}\,\mathrm{E}\left(\gamma^{*}\mathcal{S}\mathcal{S}^{*}\gamma\right). \tag{8}$$

Since the $n \times n$ matrix

$$\widehat{\mathbf{R}} \triangleq \frac{1}{T}\sum_{\tau=t}^{t+T-1} \mathbf{X}(\tau)\mathbf{X}^{*}(\tau)$$

is a scalar multiple of the sum of T matrices each having rank one, the rank of $\widehat{\mathbf{R}}$ is at most T. Therefore, when the number of snapshots T is smaller than n, the number of sensors, $\widehat{\mathbf{R}}$ is necessarily singular, thus rendering equation (7) useless (Capon, 1969).

In practice, however, when $T < n$, white-noise stabilization (diagonal loading) is applied to obtain the invertibility for $\widehat{\mathbf{R}}$ (Capon, 1969). The method calls for adding to $\widehat{\mathbf{R}}$ (prior to inverting) a diagonal matrix that can be written in the form

$$\Gamma\,\frac{\operatorname{tr}\left(\widehat{\mathbf{R}}\right)}{n}\,\mathbf{I},$$

where tr is the trace operator, $\mathbf{I}$ the identity matrix, and the stabilization factor Γ is typically chosen between 0.001 to 0.1 (Tran, 1990). Notice that a stabilization factor 0.001 corresponds to adding to the system a white sensor noise 30 dB below the average sensor power level.

The JASON algorithm (Rothaus, 1991) offers an alternative to the white-noise stabilization method in solving the constrained optimization problem (5), or (6), when the number of snapshots is less than the number of sensors. The algorithm is based on the observation that if a point source is present in the direction specified by γ, and if the noise-plus-interference vector

$$\mathbf{M}(\tau) \triangleq \mathbf{N}(\tau) + \sum_{j=1}^{k} Q_j(\tau)\beta_j \tag{9}$$

in the snapshot $\mathbf{X}(\tau)$, for $\tau = t, \ldots, t+T-1$, has all mean values zero, then the desired weight vector $\mathbf{w}$ lies in the range space of $\mathrm{E}\left(\mathcal{S}^{*}\mathcal{S}\right)$. To show this, we let $\gamma = \alpha$, where α is the steering vector of a point source with acoustic pressures $P(t), \ldots, P(t+T-1)$. Let

$$\mathcal{M}(t) \triangleq \mathcal{N}(t) + \sum_{j=1}^{k} \beta_j \mathcal{Q}_j^{*}(t).$$

Then

$$\mathbf{w}^*\mathrm{E}(\mathcal{S}\mathcal{S}^*)\mathbf{w} \;=\; \mathbf{w}^*\mathrm{E}(\mathcal{M}\mathcal{M}^*)\mathbf{w} + \mathrm{E}(\mathcal{P}^*\mathcal{P})\,|\mathbf{w}^*\alpha|^2.$$

Since $\mathrm{E}(\mathcal{M}\mathcal{M}^*)$ is positive semidefinite, and since the scalar $\mathrm{E}(\mathcal{P}^*\mathcal{P}) > 0$ (signal present), the assumption that $\mathbf{w}$ belongs to the null space of $\mathrm{E}(\mathcal{S}^*\mathcal{S})$, that is $\mathrm{E}(\mathcal{S}^*\mathcal{S})\,\mathbf{w} = \mathbf{0}$, implies immediately $\mathbf{w}^*\alpha = 0$. Therefore, to satisfy problem (5) with $\gamma = \alpha$, the weight vector $\mathbf{w}$ must lie in the range space of $\mathrm{E}(\mathcal{S}\mathcal{S}^*)$.

Operationally, the range space of $\mathrm{E}(\mathcal{S}\mathcal{S}^*)$ can be taken to be the space spanned by the columns of $\mathcal{S}$, that is the observation space. Therefore, the JASON algorithm solves the constrained optimization problem (6) with an additional requirement

$$\mathbf{w} \text{ belongs to the observation space.} \tag{10}$$

Consequently, we can represent the weight vector $\mathbf{w}$ as a linear combination of T snapshots. That is,

$$\mathbf{w} \;=\; \mathcal{S}\mathbf{c},$$

where $\mathbf{c}$ is the vector of size T whose entries are linear combination coefficients. Thus, instead of solving problem (6) for the weight vector $\mathbf{w}$, one solves the following transformed problem for the coefficient vector $\mathbf{c}$

$$\min_{\mathbf{c}}\ \mathbf{c}^*\mathcal{S}^*\mathcal{S}\mathcal{S}^*\mathcal{S}\mathbf{c} \qquad \text{subject to} \quad \mathbf{c}^*\mathcal{S}^*\gamma \;=\; 1. \tag{11}$$

The optimal solution is

$$\mathbf{c} \;=\; \frac{(\mathcal{S}^*\mathcal{S})^{-2}\,\mathcal{S}^*\gamma}{\gamma^*\mathcal{S}\,(\mathcal{S}^*\mathcal{S})^{-2}\,\mathcal{S}^*\gamma},$$

which yields the estimated output power corresponding to T snapshots

$$\mathbf{w}^*\widehat{\mathbf{R}}\mathbf{w} \;=\; \frac{1}{T}\,\frac{1}{\gamma^*\mathcal{S}\,(\mathcal{S}^*\mathcal{S})^{-2}\,\mathcal{S}^*\gamma}. \tag{12}$$

The "true" output power of the JASON algorithm corresponding to T snapshots is given by

$$\mathrm{POWER_{JASON}} \;=\; \frac{1}{T}\,\mathrm{E}\left(\frac{1}{\gamma^*\mathcal{S}\,(\mathcal{S}^*\mathcal{S})^{-2}\,\mathcal{S}^*\gamma}\right). \tag{13}$$

Notice that the $T \times T$ matrix $\mathcal{S}^*\mathcal{S}$ is invertible since the T snapshots are linearly independent.

The advantage of the JASON algorithm lies in the invertibility of $\mathcal{S}^*\mathcal{S}$, in contrast to the singularity of the matrix $\mathcal{S}\mathcal{S}^*$, when the number of snapshots T is less than the number of sensors n. Furthermore, when $T \ll n$, as in the case of a populated array, inverting the $T \times T$ matrix $\mathcal{S}^*\mathcal{S}$ is less a computational burden than inverting any $n \times n$ matrix obtained from $\mathcal{S}\mathcal{S}^*$ via diagonal modification.

4.0 SIMULATION MODEL

In this section, the general model in section 2.0 is refined for simulation. In particular, we consider an environment consisting of 20 narrowband, plane-wave sources, corrupted by additive noise, impinging on a uniform line array of 100 elements with interelement spacing equal to one-half of the wavelength. Operational details of the simulation are also presented in this section.

For the snapshot,

$$\mathbf{X}(t) \;=\; \mathbf{N}(t) \;+\; P(t)\alpha \;+\; \sum_{j=1}^{k} Q_j(t)\beta_j, \tag{14}$$

we wish to model noise vector $\mathbf{N}(t)$, direction vectors α, β_j, $j = 1,\ldots,k$, and the corresponding complex magnitudes $P(t)$, $Q_j(t)$, $j = 1,2,\ldots,k$.

Such modeling will be applied to the T consecutive snapshots $\mathbf{X}(t)$, $\mathbf{X}(t+1)$, $\ldots$, $\mathbf{X}(t+T-1)$, as in

$$\mathcal{S}(t) \;=\; \mathcal{N}(t) \;+\; \alpha\mathcal{P}^*(t) \;+\; \sum_{j=1}^{k} \beta_j \mathcal{Q}_j^*(t), \tag{15}$$

where we recall

$$\begin{aligned} \mathcal{S}(t) &\triangleq \Big[\mathbf{X}(t) \,\vdots\, \mathbf{X}(t+1) \,\vdots\, \cdots \,\vdots\, \mathbf{X}(t+T-1)\Big], \\ \mathcal{N}(t) &\triangleq \Big[\mathbf{N}(t) \,\vdots\, \mathbf{N}(t+1) \,\cdots\, \vdots\, \mathbf{N}(t+T-1)\Big], \end{aligned} \tag{16}$$

and

$$\mathcal{P}(t) \triangleq \begin{bmatrix} \overline{P}(t) \\ \overline{P}(t+1) \\ \vdots \\ \overline{P}(t+T-1) \end{bmatrix}, \qquad \mathcal{Q}_j(t) \triangleq \begin{bmatrix} \overline{Q_j}(t) \\ \overline{Q_j}(t+1) \\ \vdots \\ \overline{Q_j}(t+T-1) \end{bmatrix}, \quad j = 1,2,\cdots,k.$$

We shall consider the case where sources located in the farfield can be modeled as plane waves. Also, for simplicity we shall consider a line array of n elements, uniformly distributed with interelement spacing equal to one-half of the array wavelength.

For a line array, the angle-of-arrival of a plane wave is measured relative to the normal to the array. Consequently, the range of the angle-of-arrival is -90^0 to 90^0.

We recall the following useful result (Haykin, 1985). For the coordinate reference at the center of the array, the direction vector of a plane wave impinging on the uniform linear array of n elements at an angle-of-arrival ϕ, measured with respect to the normal to the array, is given by

$$\left[e^{-\mathrm{i}(\frac{n-1}{2})\omega},\ldots,e^{-\mathrm{i}\frac{1}{2}\omega},\ e^{\mathrm{i}\frac{1}{2}\omega},\ldots,e^{-\mathrm{i}(\frac{n-1}{2})\omega}\right]^T, \qquad n \text{ even},$$

$$\left[e^{-\mathrm{i}(\frac{n-1}{2})\omega},\ldots,e^{-\mathrm{i}\omega},\ 1,\ e^{\mathrm{i}\omega},\ldots,e^{-\mathrm{i}(\frac{n-1}{2})\omega}\right]^T, \qquad n \text{ odd},$$

where superscript T stands for transpose, $\mathrm{i} = \sqrt{-1}$, and

$$\omega = \frac{2\pi d}{\lambda}\sin(\phi)$$

with d as the interelement spacing and λ the array wavelength. Note that the "center" of the array is its actual middle sensor if n is odd, otherwise it is a fictitious center. Therefore, with the coordinate reference at the center of the array, the direction vector of a plane wave impinging on the uniform linear array can be obtained readily by setting $d = \lambda/2$.

In the following we will realize $\mathcal{N}(t)$, $\mathcal{P}(t)$, $\mathcal{Q}_j(t)$, $j = 1,\ldots,k$, using normally distributed random numbers available in the MATLAB package.

The function `rand(n,T)` in MATLAB generates an $(n \times T)$-matrix with random entries. By specifying the function `rand` as `normal` beforehand, the entries of the resulting matrix will be normally distributed with mean 0.0 and variance 1.0. Similarly,

$$\mathtt{rand(n,T)} + \mathrm{i}\ \mathtt{rand(n,T)} \tag{17}$$

generates a complex random matrix of size $n \times T$ whose real part and imaginary part of each of the entries are normally distributed with means 0.0 and variances 1.0. This can be taken as a prototype for $\mathcal{N}(t)$ and, similarly,

$$\mathtt{rand(T,1)} + \mathrm{i}\,\mathtt{rand(T,1)} \tag{18}$$

for $\mathcal{P}(t)$, and $\mathcal{Q}_j(t), j = 1, \ldots, k$. Observe that the complex vector in expression (18) and columns of the complex matrix in (17) are realizations of zero mean, complex Gaussian random vectors.

For simulation we wish to generate $\mathcal{N}(t)$, $\mathcal{P}(t)$, $\mathcal{Q}_j(t)$, $j = 1, \ldots, k$, as random matrices with zero means and with average noise power per sensor σ_n^2, average signal power σ_s^2, and average power of the j-th interference σ_j^2, where we recall,

$$\sigma_n^2 \triangleq \frac{1}{n}\,\mathrm{tr}\left(\frac{1}{T}\,\mathcal{N}(t)\mathcal{N}^*(t)\right) = \frac{1}{nT}\,\mathrm{tr}\,(\mathcal{N}(t)\mathcal{N}^*(t)),$$

$$\sigma_s^2 \triangleq \frac{1}{T}\,\mathcal{P}^*(t)\mathcal{P}(t), \qquad \sigma_j^2 \triangleq \frac{1}{T}\,\mathcal{Q}_j^*(t)\mathcal{Q}_j(t), \quad j = 1, 2, \ldots, k.$$

Furthermore, for simplicity we choose $\sigma_n^2 = 1$.

For any matrix $\mathbf{A} = (a_{ij})$, recall that

$$\mathrm{tr}\,(\mathbf{A}\mathbf{A}^*) = \sum_{i,j} |a_{ij}|^2 = \|\mathbf{A}\|_{\mathrm{F}}^2,$$

where $\|\mathbf{A}\|_{\mathrm{F}}$ denotes the Frobenius norm of $\mathbf{A}$. In particular, we can write

$$\sigma_n^2 = \frac{1}{nT}\,\|\mathcal{N}(t)\|_{\mathrm{F}}^2.$$

Consider the normalization

$$\mathcal{N}(t) = \frac{\sqrt{nT}\,(\mathtt{rand(n,T)} + \mathrm{i}\,\mathtt{rand(n,T)})}{\|\mathtt{rand(n,T)} + \mathrm{i}\,\mathtt{rand(n,T)}\|_{\mathrm{F}}} \tag{19}$$

Then the average noise power is unity.

Strictly speaking, the noise is no longer Gaussian since the denominator of equation (19) is randomly distributed. The distribution of $\|\mathtt{rand(n,T)} + \mathrm{i}\,\mathtt{rand(n,T)}\|_{\mathrm{F}}$ depends largely on the statistical independence (or dependence) of the $2nT$ normally distributed random variables (each with mean 0.0 and variance 1.0) that make up the real and imaginary parts of entries of the matrix $\mathtt{rand(n,T)} + \mathrm{i}\,\mathtt{rand(n,T)}$. In the ideal situation where they are statistically independent, then the denominator of (19) has the chi distribution (Melsa & Sage, 1973, pp. 314-315).

Without precise knowledge of the distribution of $\|\mathrm{rand(n,T)} + \mathrm{i}\ \mathrm{rand(n,T)}\|_{\mathrm{F}}$; however, for practical purposes, we may assume its expectation exists and is greater than zero. The assumption on the positivity of the expected value of the denominator of equation (19) is justified since $\|\mathrm{rand(n,T)} + \mathrm{i}\ \mathrm{rand(n,T)}\|_{\mathrm{F}}$ represents a "magnitude-type" quantity as signified by the definition of Frobenius norm. Consequently,

$$\mathrm{E}\left(\frac{\sqrt{nT}\ (\mathrm{rand(n,T)} + \mathrm{i}\ \mathrm{rand(n,T)})}{\|\mathrm{rand(n,T)} + \mathrm{i}\ \mathrm{rand(n,T)}\|_{\mathrm{F}}}\right) \approx \frac{\mathrm{E}\left(\sqrt{nT}\ (\mathrm{rand(n,T)} + \mathrm{i}\ \mathrm{rand(n,T)})\right)}{\mathrm{E}\left(\|\mathrm{rand(n,T)} + \mathrm{i}\ \mathrm{rand(n,T)}\|_{\mathrm{F}}\right)} = \mathbf{0}_{n\times T},$$

that is, $\mathcal{N}(t)$ is a complex random matrix with mean $\mathbf{0}_{n\times T}$.

In view of equation (16), the noise is zero mean. Furthermore, it is colored since it may be temporally correlated from sample to sample.

Similarly, we consider

$$\mathcal{P}(t) = \frac{\sqrt{\sigma_s^2\, T}\ (\mathrm{rand(T,1)} + \mathrm{i}\ \mathrm{rand(T,1)})}{\|\mathrm{rand(T,1)} + \mathrm{i}\ \mathrm{rand(T,1)}\|}, \tag{20}$$

where $\|\cdot\|$ stands for the usual Euclidean norm, a special case of the Frobenius norm. Then $\frac{1}{T}\ \mathcal{P}^*(t)\mathcal{P}(t) = \sigma_s^2$. Moreover, it follows from the above argument that $\mathcal{P}(t)$ is a complex random vector with mean $\mathbf{0}_{T\times 1}$.

Finally, $\mathcal{Q}_j(t)$, $j = 1, \ldots, k$, can be generated by

$$\mathcal{Q}_j(t) = \frac{\sqrt{\sigma_j^2\, T}\ (\mathrm{rand(T,1)} + \mathrm{i}\ \mathrm{rand(T,1)})}{\|\mathrm{rand(T,1)} + \mathrm{i}\ \mathrm{rand(T,1)}\|}. \tag{21}$$

As a consequence of the modeling of equations (19), (20) and (21), for any source chosen as the desired signal, the noise-plus-interference vector $\mathbf{M}(\tau) \triangleq \mathbf{N}(\tau) + \sum_{j=1}^{k} Q_j(\tau)\beta_j$ of the data snapshot $\mathbf{X}(\tau)$, for $\tau = t, \ldots, t+T-1$, has all mean values of zero.

For illustration, an interactive MATLAB implementation for plotting array response is presented in Appendix A. This code can be run on a PC. Actual simulations, however, were done on a CONVEX C220, a two-processor minisupercomputer at the Naval Ocean Systems Center.

5.0 SIMULATION RESULTS

In this section, we describe the multisource environment used in simulation together with qualitative and quantitative results concerning properties and performance of conventional, MVDR (with stabilization factors 0.001, 0.01, and 0.1), and JASON beamformers when the number of snapshots is small. Qualitative results, based on output array response, and quantitative results, based on normalized output deflection and peak-to-background ratio, are presented in subsections 5.1 and 5.2, respectively.

We consider 20 sources, corrupted by additive noise, impinging on a line array of 100 equally spaced sensors with interelement spacing equal to one half of the array wavelength. The noise components $\mathbf{N}(t), \ldots, \mathbf{N}(t+T-1)$ in the T consecutive snapshots are modeled by equation (19) as being random with zero means and unit average power per sensor. Direction vectors of sources are assumed to remain constant during the processing interval indicated by the duration of the T snapshots. Acoustic pressures, or complex amplitudes, of sources are modeled as in equation (20) where average source powers are specified relative to average noise power per sensor (0 dB). Table 1 below lists source angles and the corresponding powers.

Table 1. Angle and power of 20 sources.

source	angle (deg)	source power (dB)
1	-65	-5
2	-45	-15
3	-30	-10
4	-10	5
5 - 15	10, 12, 14, 16, 18, 20, 22, 24, 26, 28, 30	0
16 - 20	40, 42, 44, 46 48	

Notice that there are two clusters of sources of 0-dB average power; the first group is comprised of 11 sources, the second of 5 sources, with 2^0 spacing in each group. This is the smallest angular separation between any 2 of the 20 sources.

The Rayleigh limit of angular resolution of a uniform linear array of n elements is approximately $2/(n-1)$ radians (Krolik & Swingler, 1989). In particular, for $n = 100$ sensors, the Rayleigh limit is approximately 1.1575^0, which is less than the 2^0 spacing just mentioned.

5.1 Qualitative Results

The array response of the conventional beamformer, of MVDR with stabilization factors $0.001, 0.01, 0.1$, and of the JASON algorithm are plotted for the look-direction steering vector sweeping from -90^0 to 90^0 with 1^0 increments. The number of snapshots considered are 10, 20, 30, 40 and 50, that is, from $\frac{1}{10}$ to $\frac{1}{2}$ of the number of elements.

Corresponding to each number of snapshots, we plotted the array response of five independent trials and, in a separate graph, the average response taken over 200 independent trials for each method. These plots of the array response provide a qualitative assessment of the properties and performance of each beamformer.

For a quick reference, figures of array response of algorithms are listed in tables 2 through 6. For example, table 2 shows that figure 1(a1) depicts conventional array response of 5 independent trials whereas figure 1(a2) exhibits the average response of the conventional beamformer taken over 200 independent trials, and that these two figures were obtained in the case where the number of snapshots $T = 10$.

Table 2. List of figures of conventional array response.

number of snapshots	10	20	30	40	50
Figure	five independent trials				
	1(a1)	1(b1)	1(c1)	1(d1)	1(e1)
	average of 200 independent trials				
	1(a2)	1(b2)	1(c2)	1(d2)	1(e2)

Table 3. List of figures of MVDR array response.
(stabilization factor 0.001).

number of snapshots	10	20	30	40	50
Figure	five independent trials				
	2(a1)	2(b1)	2(c1)	2(d1)	2(e1)
	average of 200 independent trials				
	2(a2)	2(b2)	2(c2)	2(d2)	2(e2)

Table 4. List of figures of MVDR array response.
(stabilization factor 0.01).

number of snapshots	10	20	30	40	50
Figure	five independent trials				
	3(a1)	3(b1)	3(c1)	3(d1)	3(e1)
	average of 200 independent trials				
	3(a2)	3(b2)	3(c2)	3(d2)	3(e2)

Table 5. List of figures of MVDR array response.
(stabilization factor 0.1).

number of snapshots	10	20	30	40	50
Figure	five independent trials				
	4(a1)	4(b1)	4(c1)	4(d1)	4(e1)
	average of 200 independent trials				
	4(a2)	4(b2)	4(c2)	4(d2)	4(e2)

Table 6. List of figures of JASON array response.

number of snapshots	10	20	30	40	50
Figure	five independent trials				
	5(a1)	5(b1)	5(c1)	5(d1)	5(e1)
	average of 200 independent trials				
	5(a2)	5(b2)	5(c2)	5(d2)	5(e2)

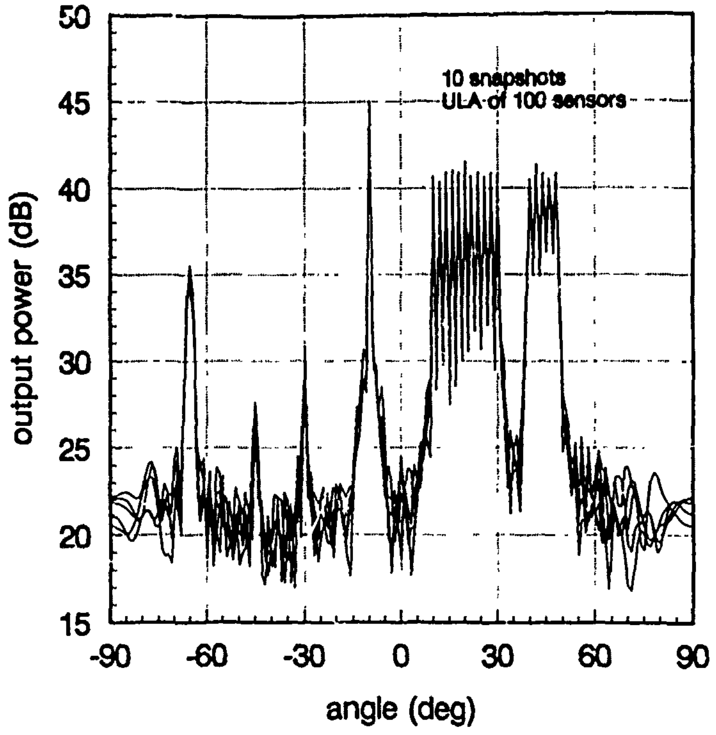

(a1) Five independent trials, each with 10 snapshots.

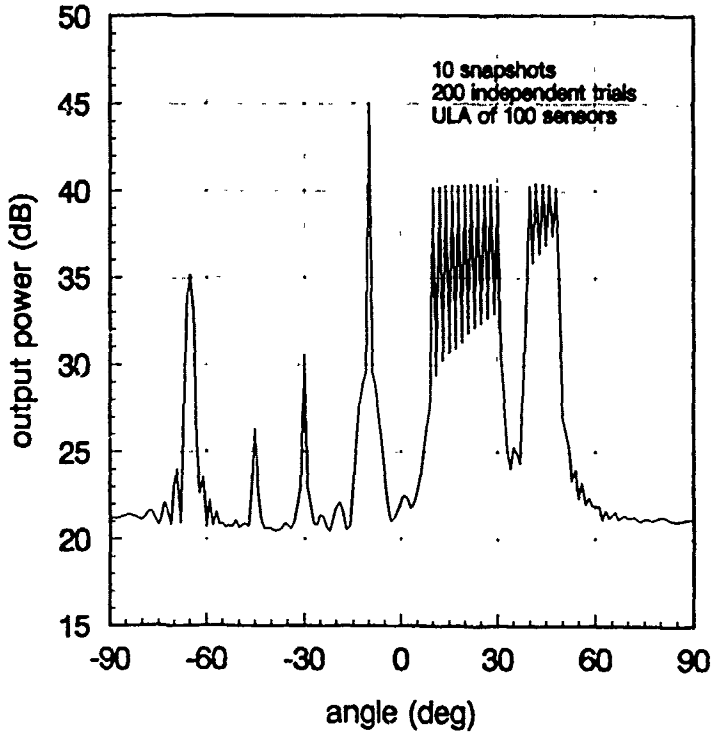

(a2) Average of 200 independent trials, each with 10 snapshots.

Figure 1. Conventional array response.

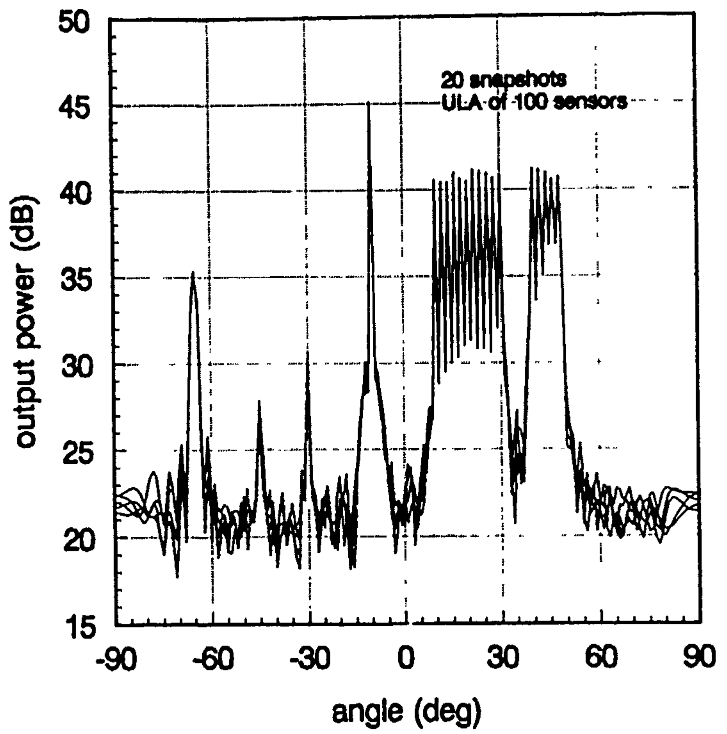

(b1) Five independent trials, each with 20 snapshots.

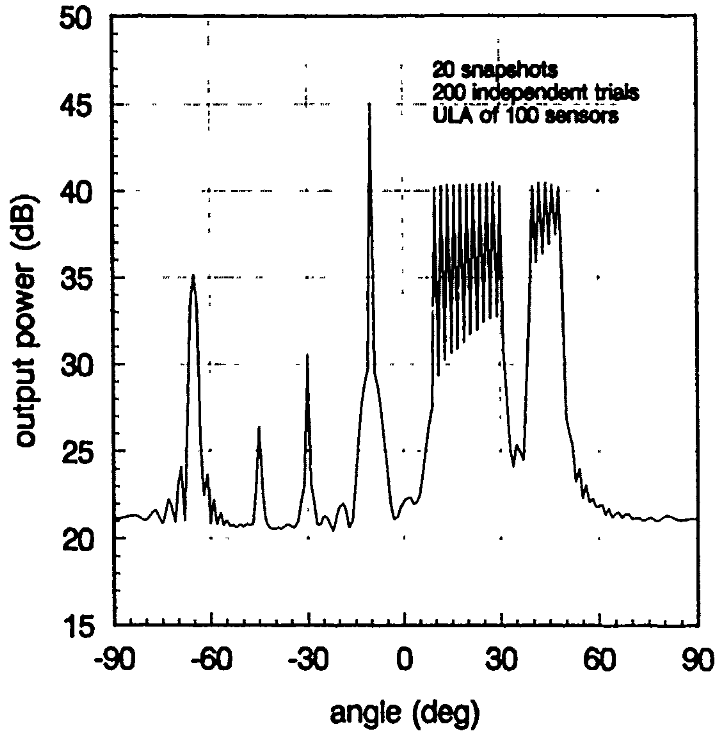

(b2) Average of 200 independent trials, each with 20 snapshots.

Figure 1 (cont.). Conventional array response.

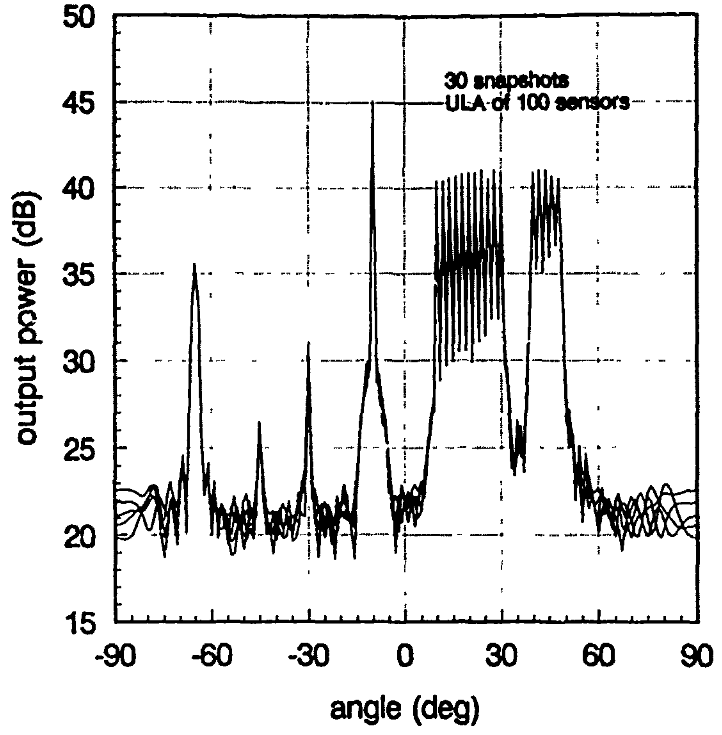

(c1) Five independent trials, each with 30 snapshots.

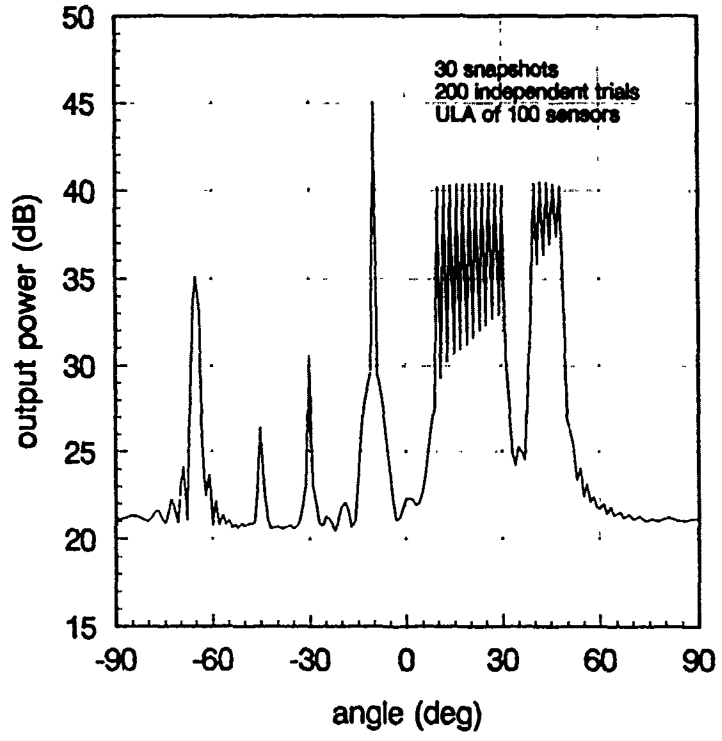

(c2) Average of 200 independent trials, each with 30 snapshots.

Figure 1 (cont.). Conventional array response.

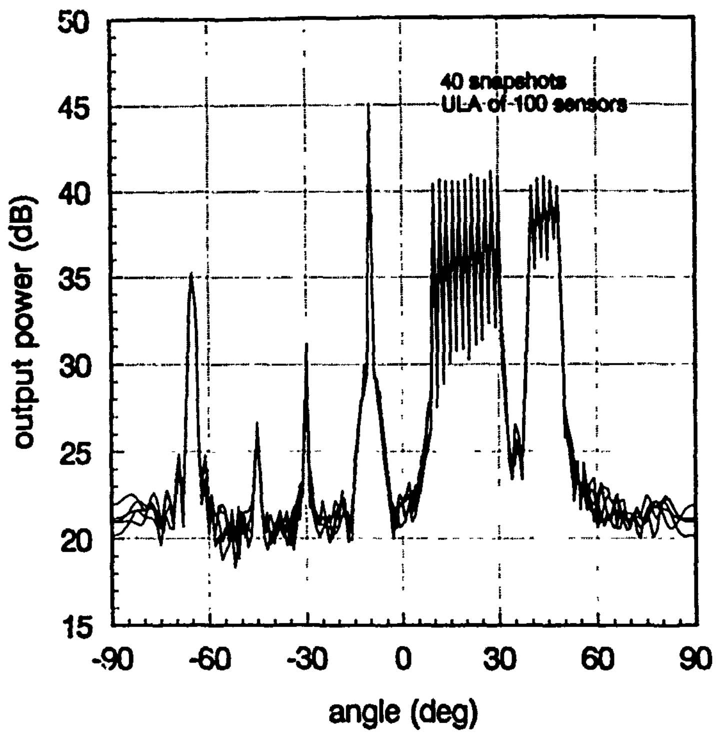

(d1) Five independent trials, each with 40 snapshots.

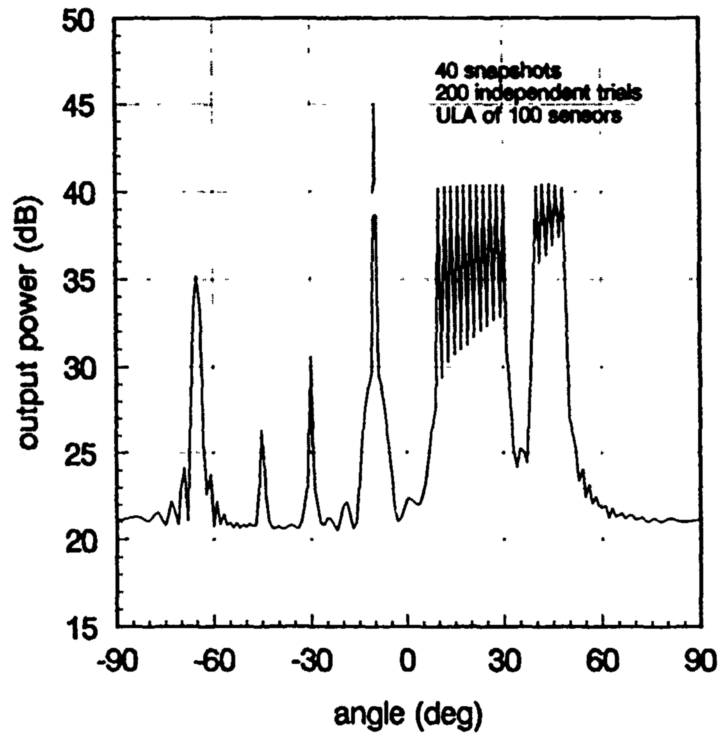

(d2) Average of 200 independent trials, each with 40 snapshots.

Figure 1 (cont.). Conventional array response.

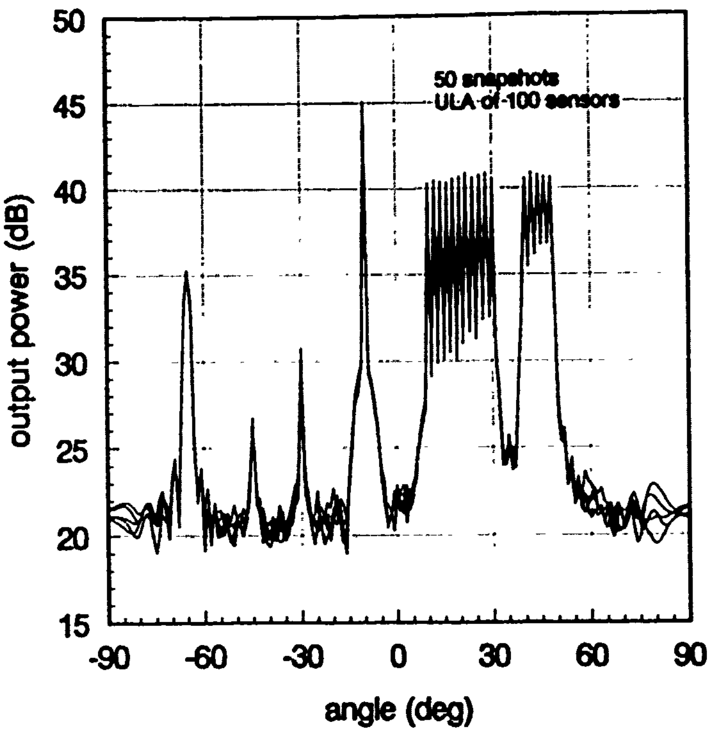

(e1) Five independent trials, each with 50 snapshots.

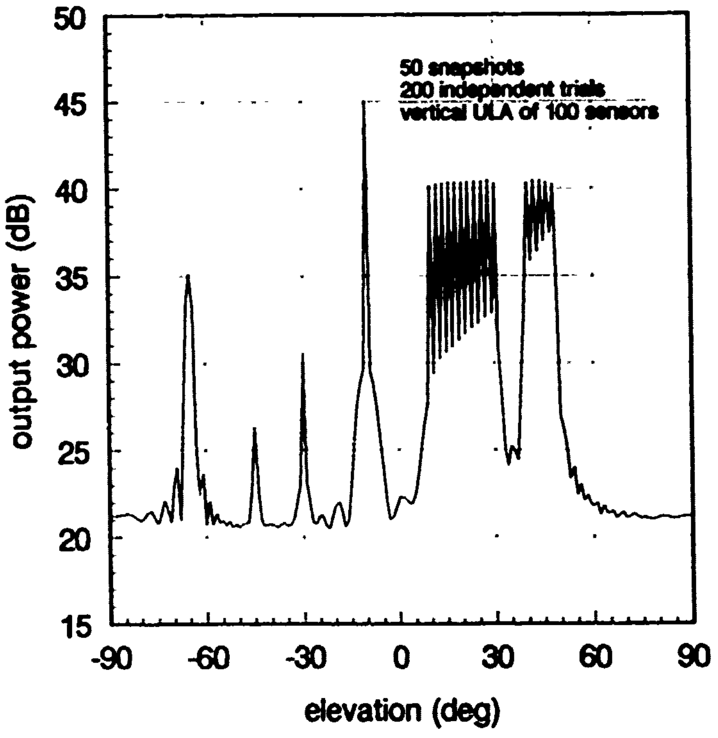

(e2) Average of 200 independent trials, each with 50 snapshots.

Figure 1 (cont.). Conventional array response.

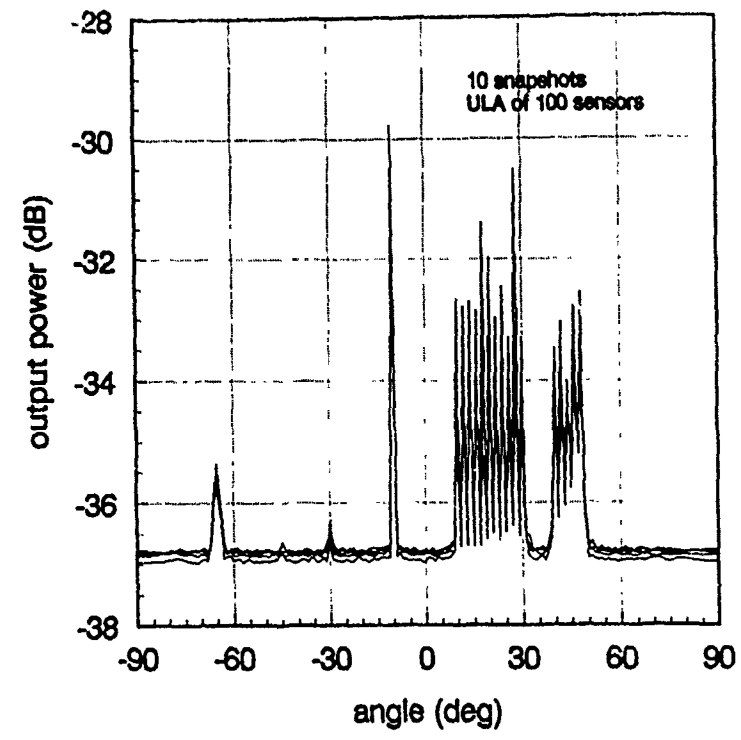

(a1) Five independent trials, each with 10 snapshots.

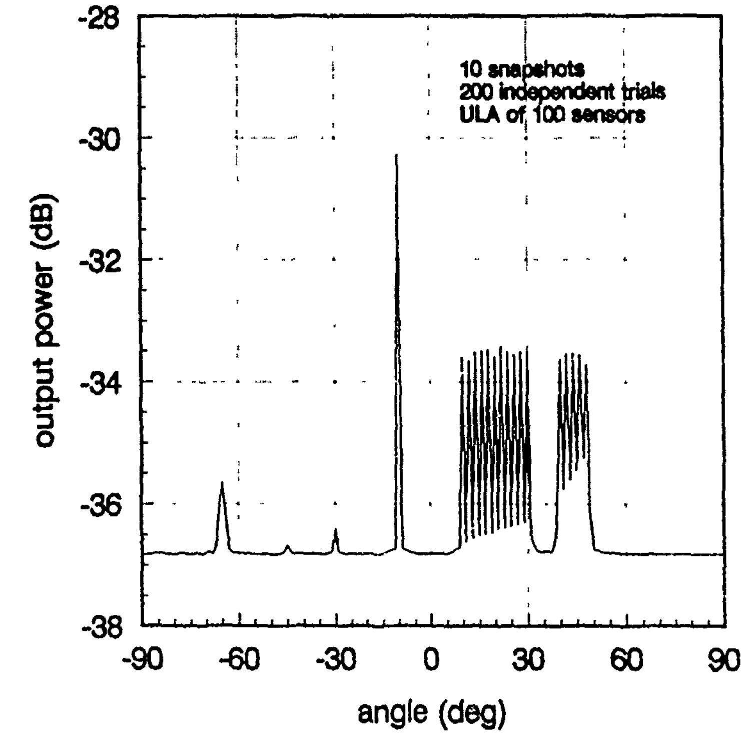

(a2) Average of 200 independent trials, each with 10 snapshots.

Figure 2. MVDR array response with stabilization factor 0.001.

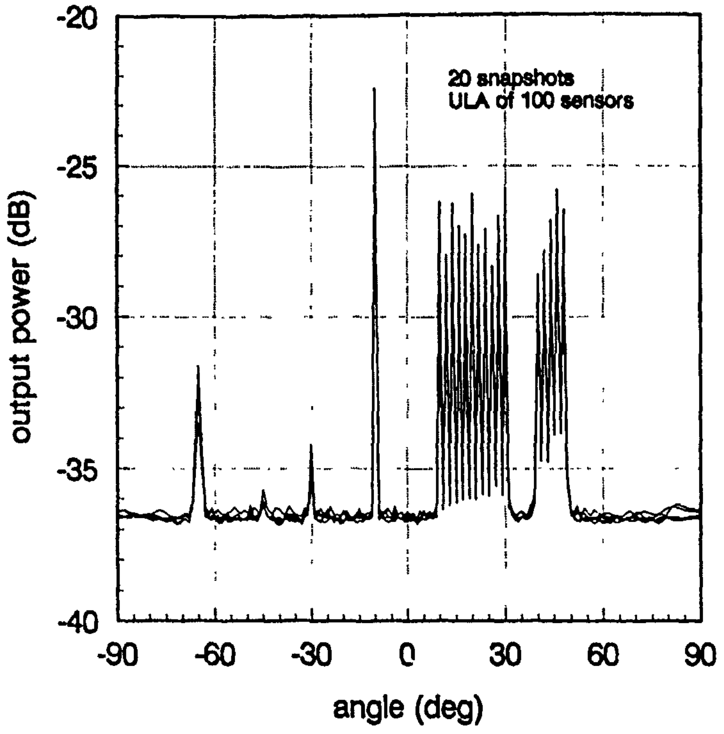

(b1) Five independent trials, each with 20 snapshots.

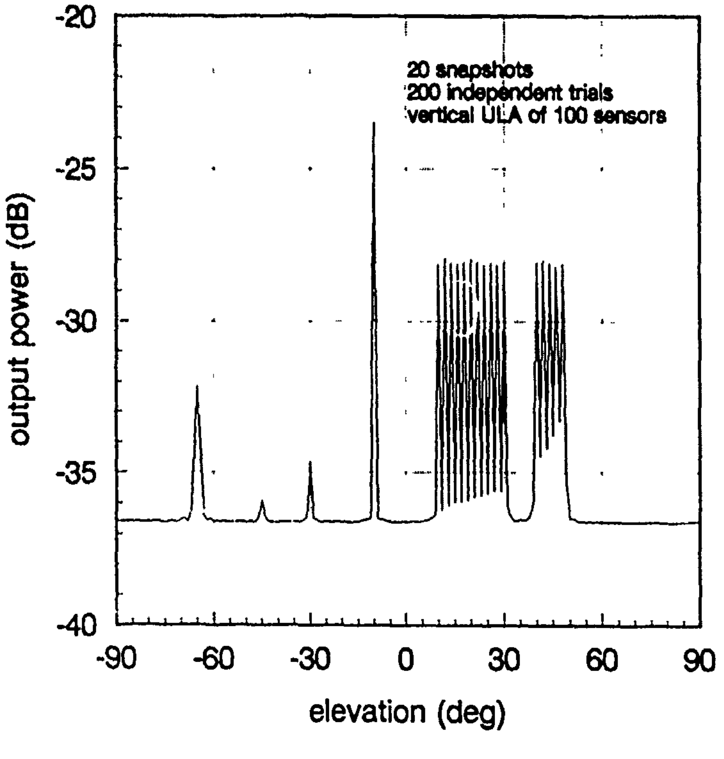

(b2) Average of 200 independent trials, each with 20 snapshots.

Figure 2 (cont.). MVDR array response with stabilization factor 0.001.

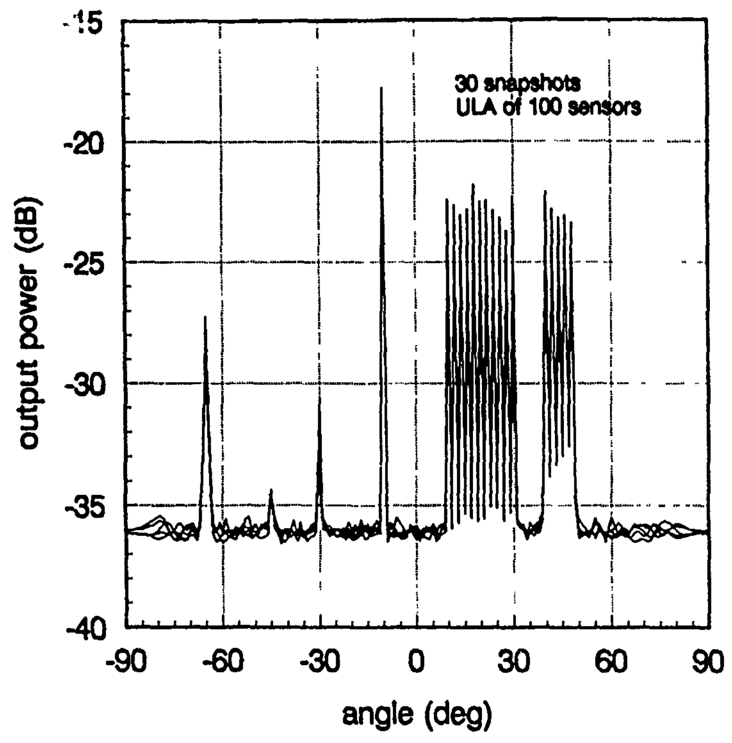

(c1) Five independent trials, each with 30 snapshots.

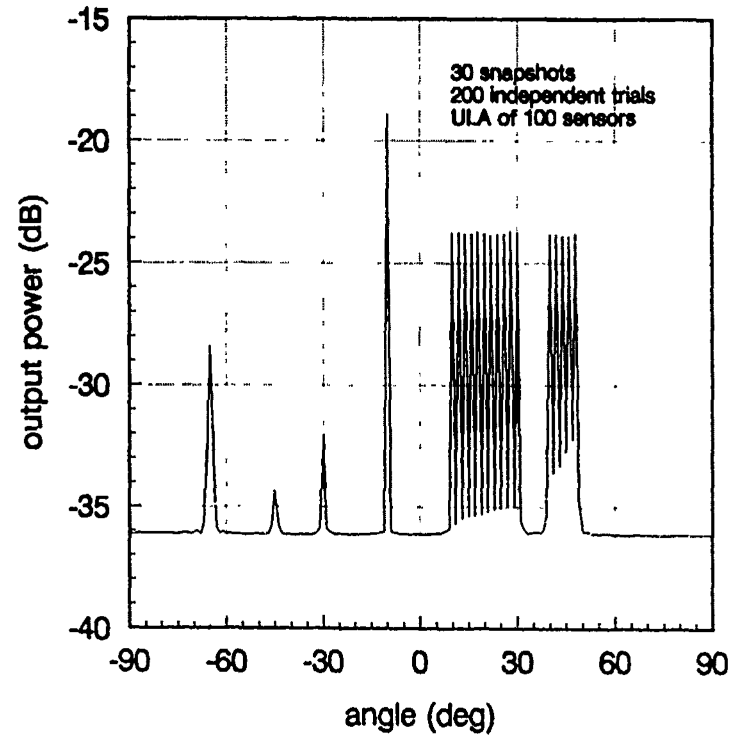

(c2) Average of 200 independent trials, each with 30 snapshots.

Figure 2 (cont.). MVDR array response with stabilization factor 0.001.

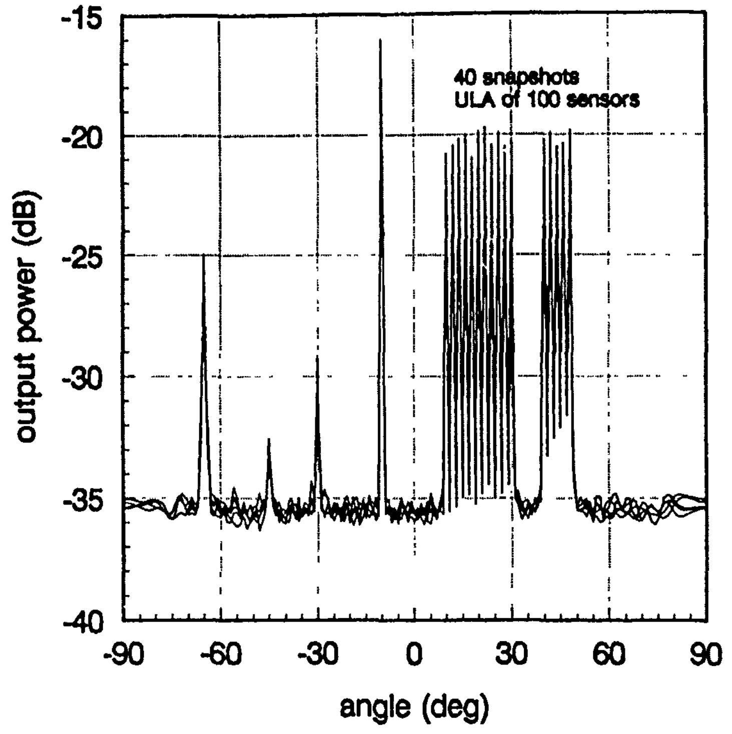

(d1) Five independent trials, each with 40 snapshots.

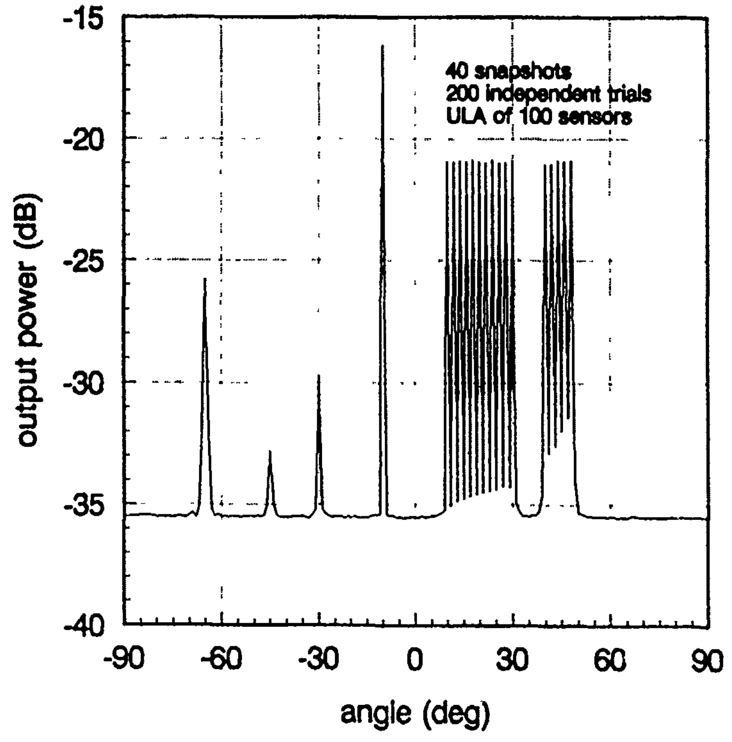

(d2) Average of 200 independent trials, each with 40 snapshots.

Figure 2 (cont.). MVDR array response with stabilization factor 0.001.

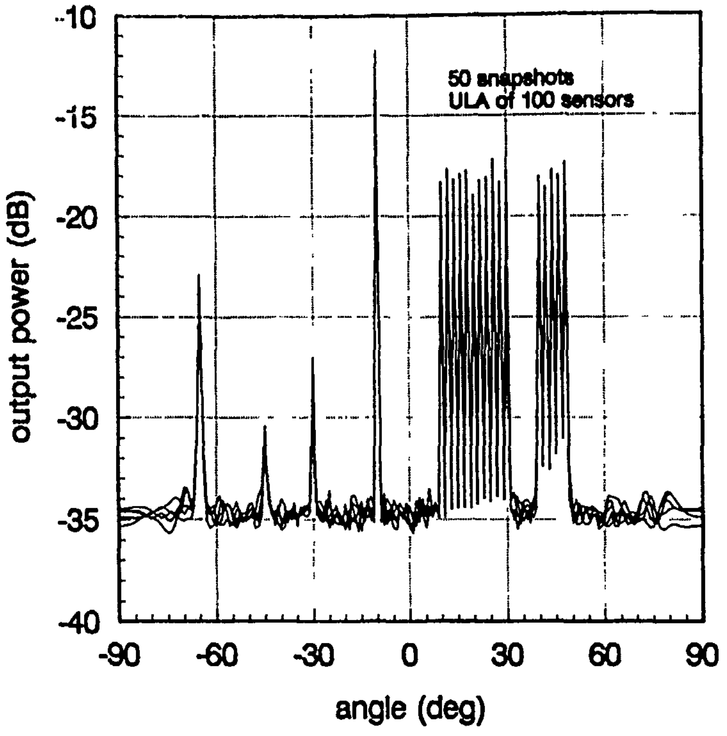

(e1) Five independent trials, each with 50 snapshots.

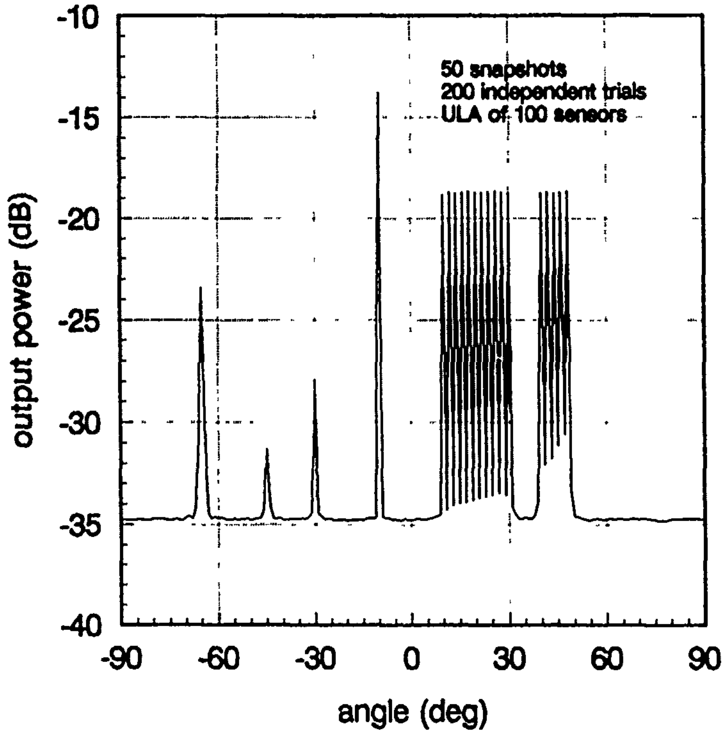

(e2) Average of 200 independent trials, each with 50 snapshots.

Figure 2 (cont.). MVDR array response with stabilization factor 0.001.

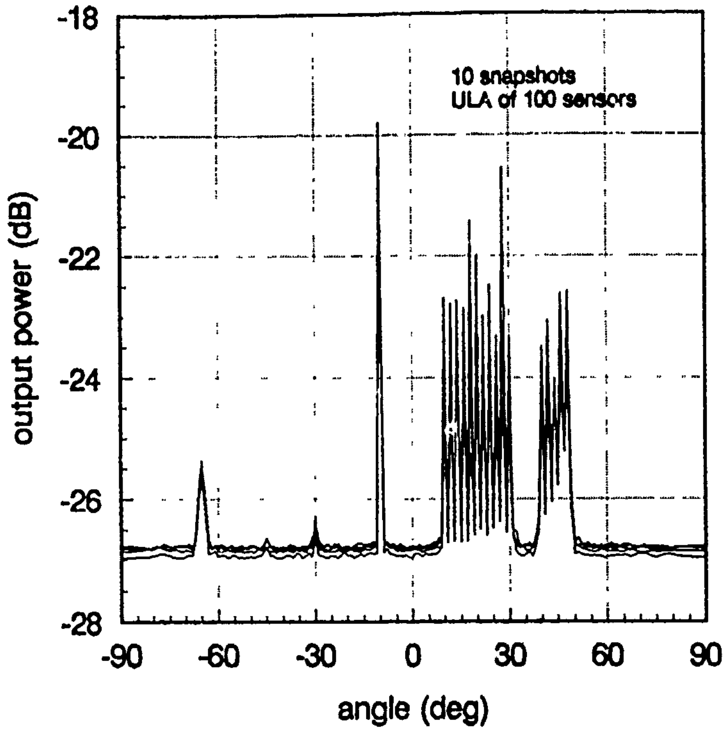

(a1) Five independent trials, each with 10 snapshots.

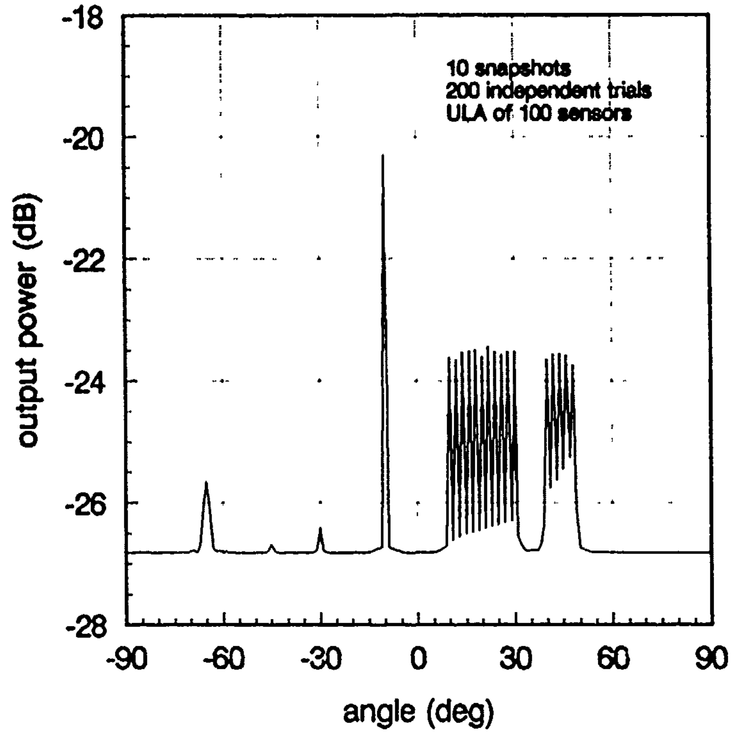

(a2) Average of 200 independent trials, each with 10 snapshots.

Figure 3. MVDR array response with stabilization factor 0.01.

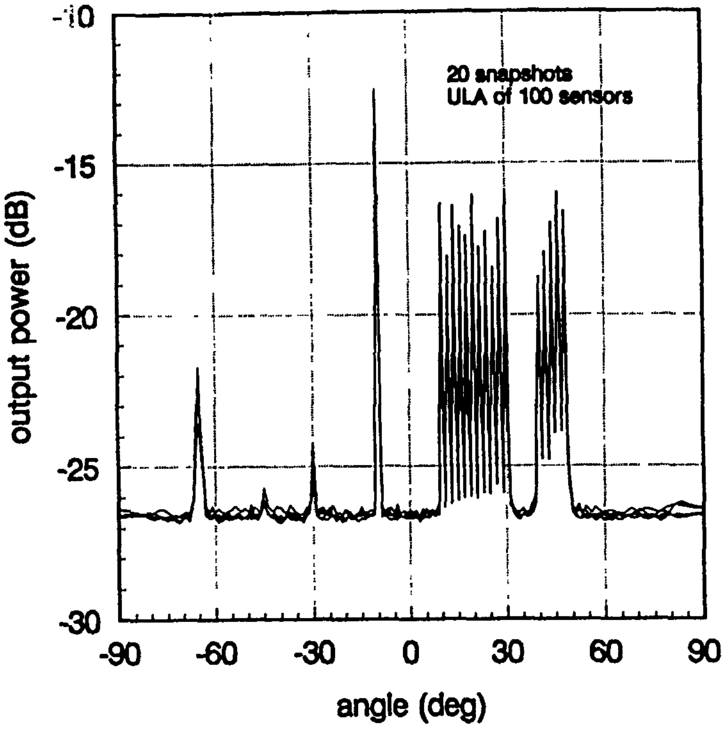

(b1) Five independent trials, each with 20 snapshots.

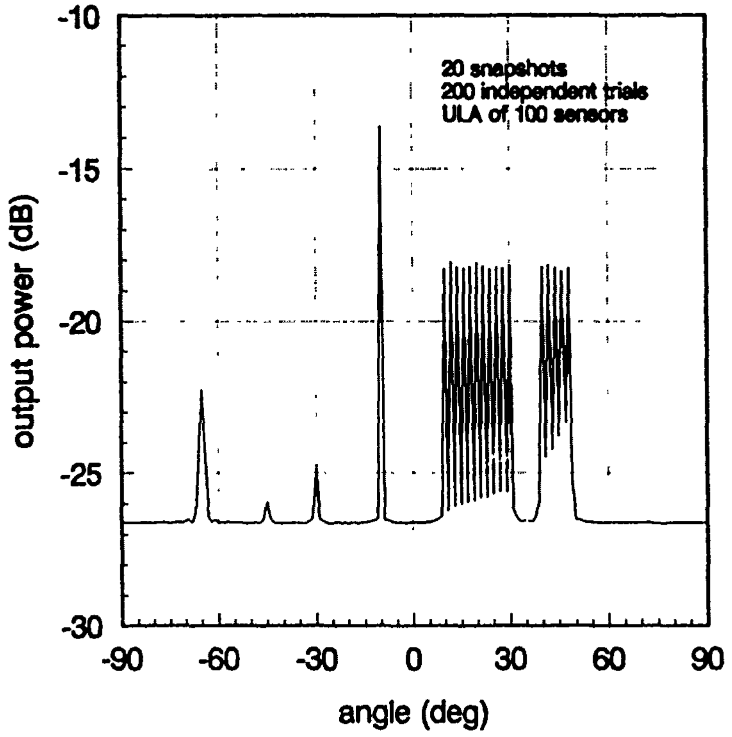

(b2) Average of 200 independent trials, each with 20 snapshots.

Figure 3 (cont.). MVDR array response with stabilization factor 0.01.

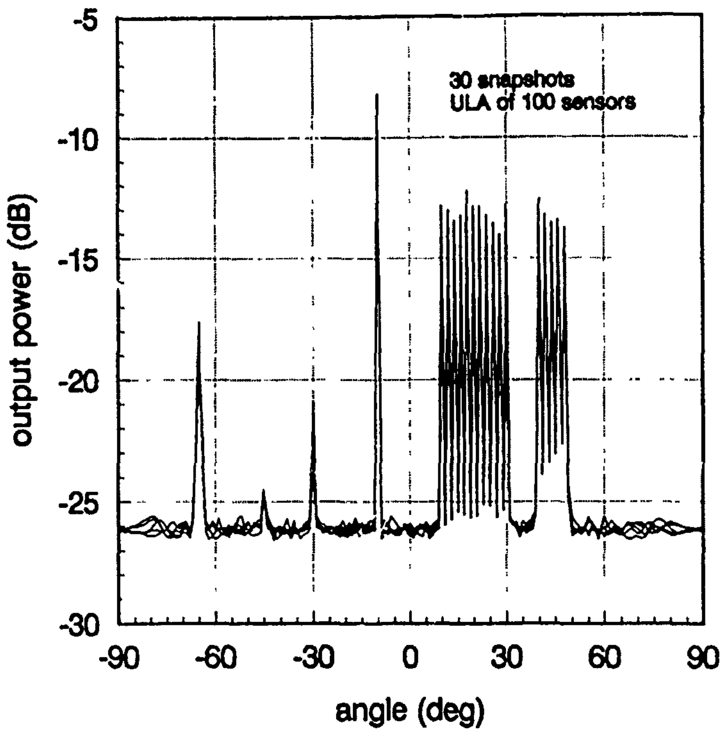

(c1) Five independent trials, each with 30 snapshots.

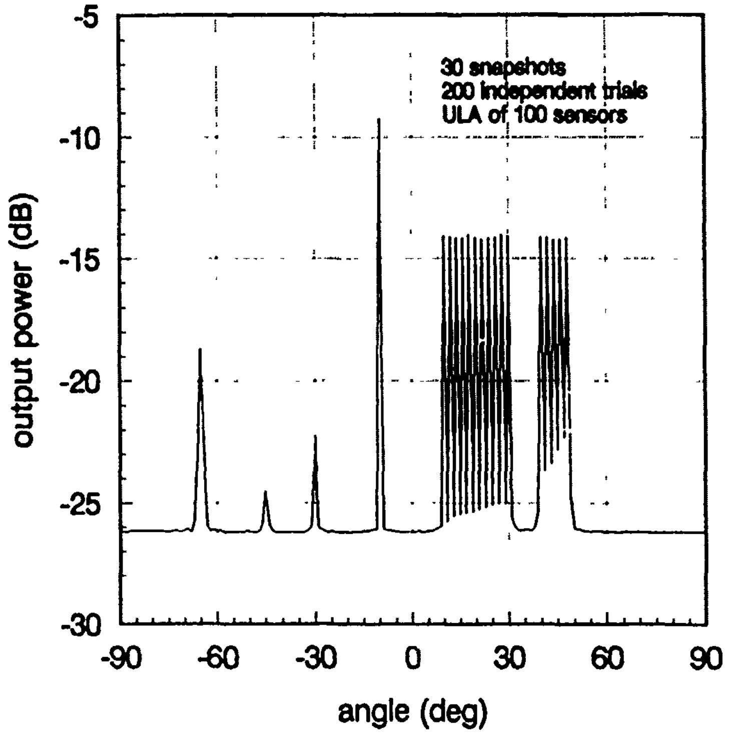

(c2) Average of 200 independent trials, each with 30 snapshots.

Figure 3 (cont.). MVDR array response with stabilization factor 0.01.

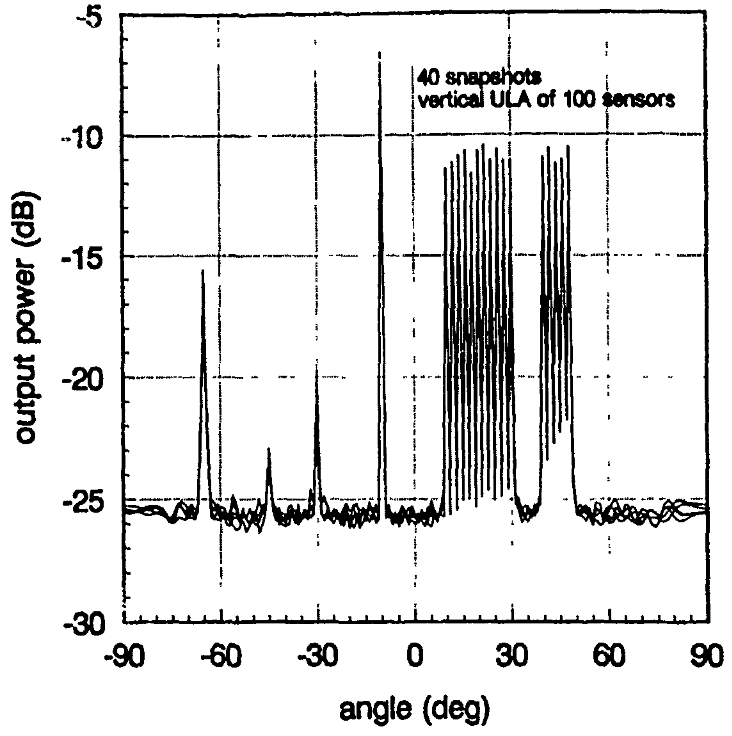

(d1) Five independent trials, each with 40 snapshots.

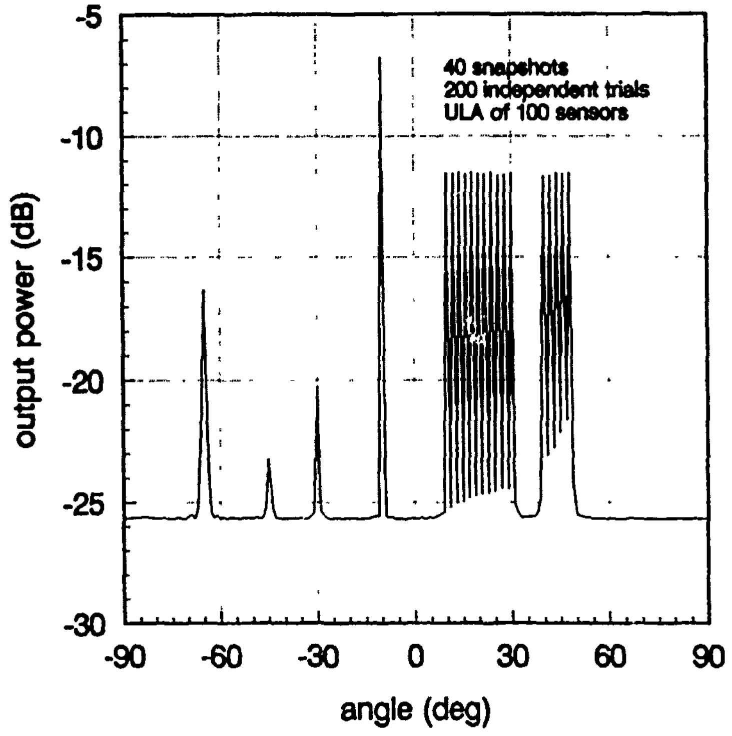

(d2) Average of 200 independent trials, each with 40 snapshots.

Figure 3 (cont.). MVDR array response with stabilization factor 0.01.

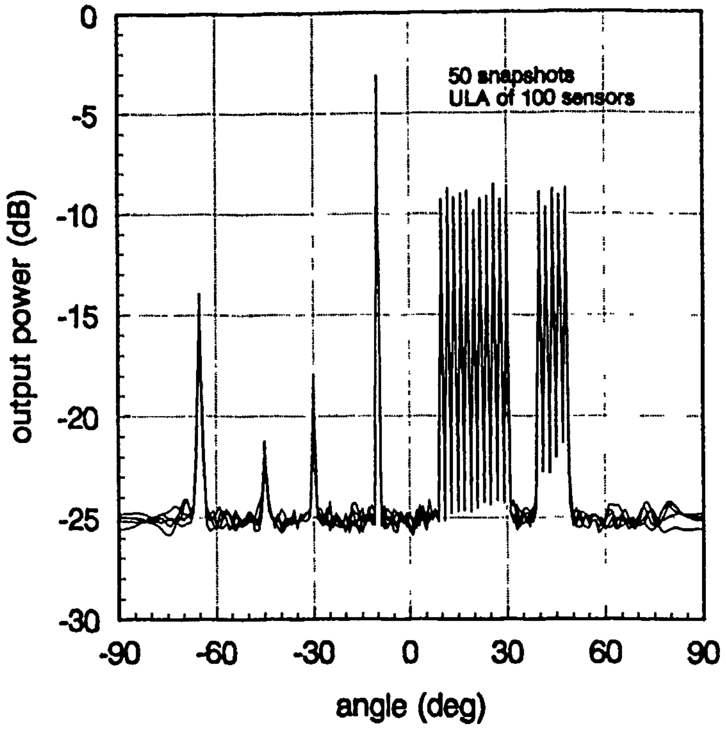

(e1) Five independent trials, each with 50 snapshots.

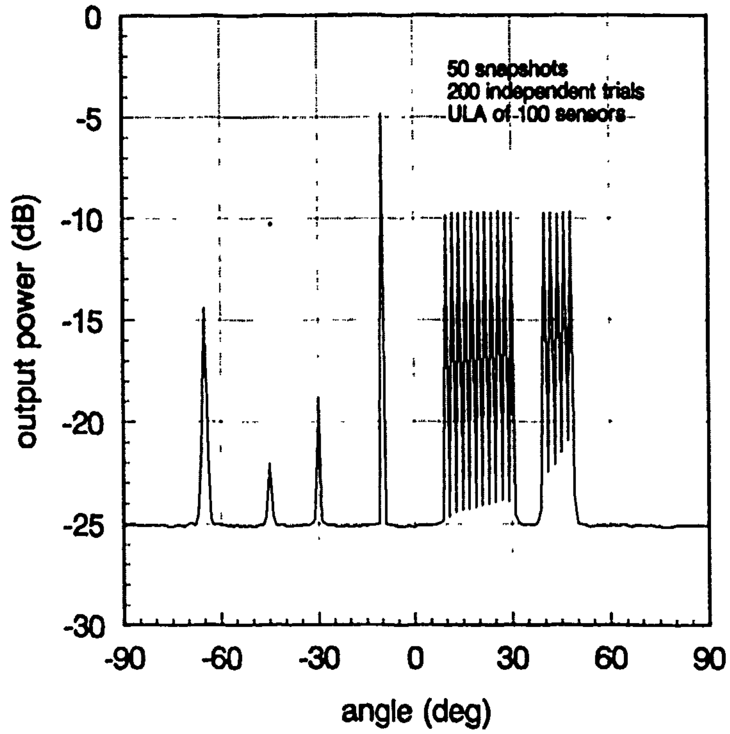

(e2) Average of 200 independent trials, each with 50 snapshots.

Figure 3 (cont.). MVDR array response with stabilization factor 0.01.

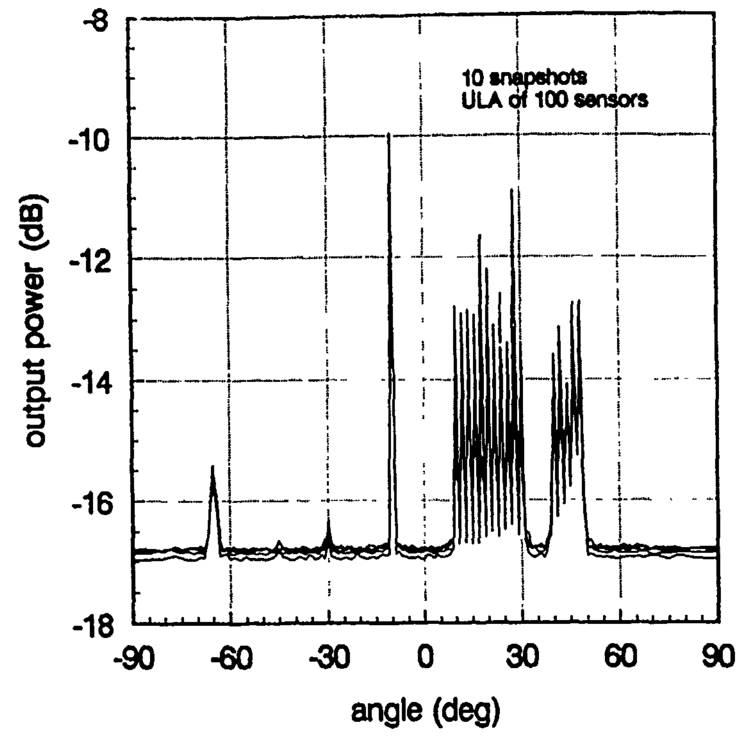

(a1) Five independent trials, each with 10 snapshots.

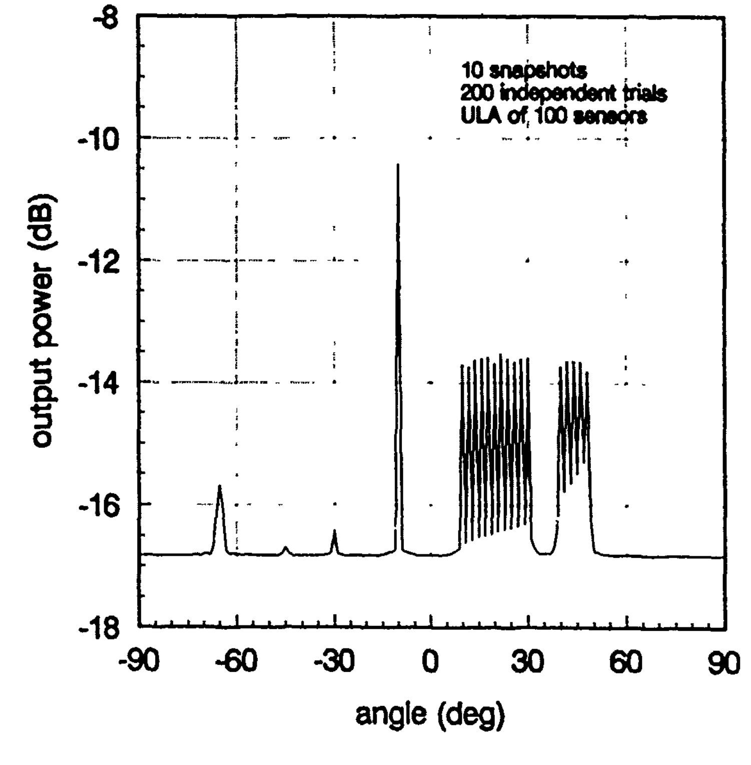

(a2) Average of 200 independent trials, each with 10 snapshots.

Figure 4. MVDR array response with stabilization factor 0.1.

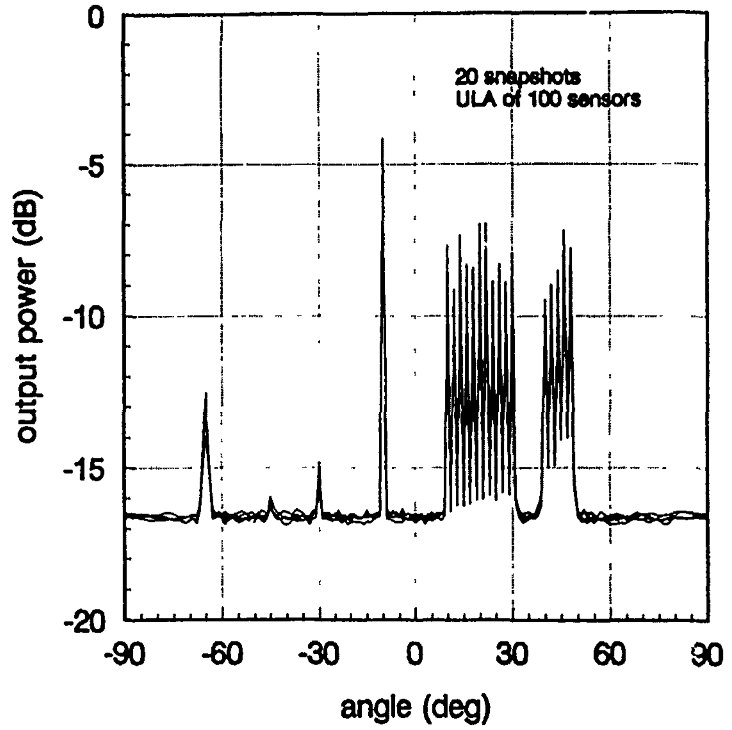

(b1) Five independent trials, each with 20 snapshots.

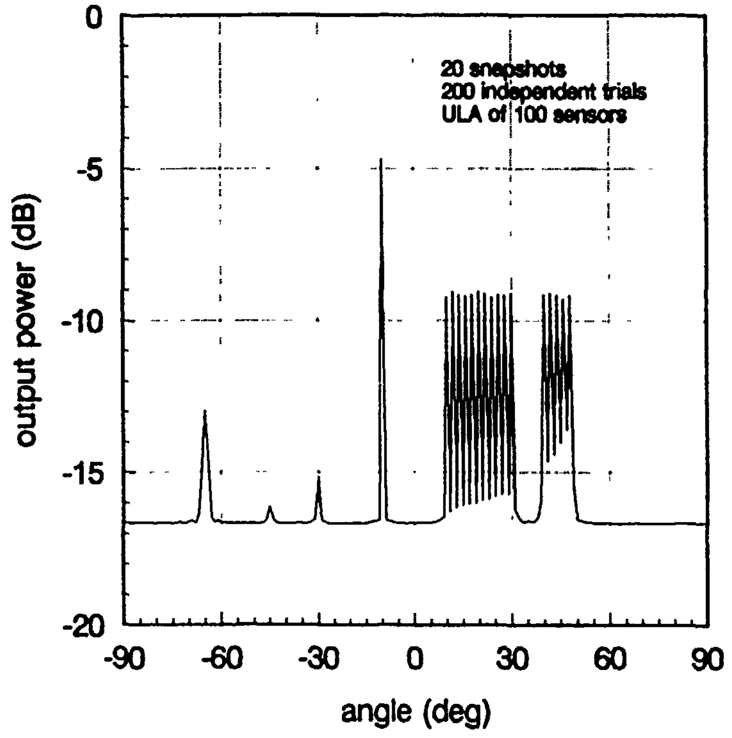

(b2) Average of 200 independent trials, each with 20 snapshots.

Figure 4 (cont.). MVDR array response with stabilization factor 0.1.

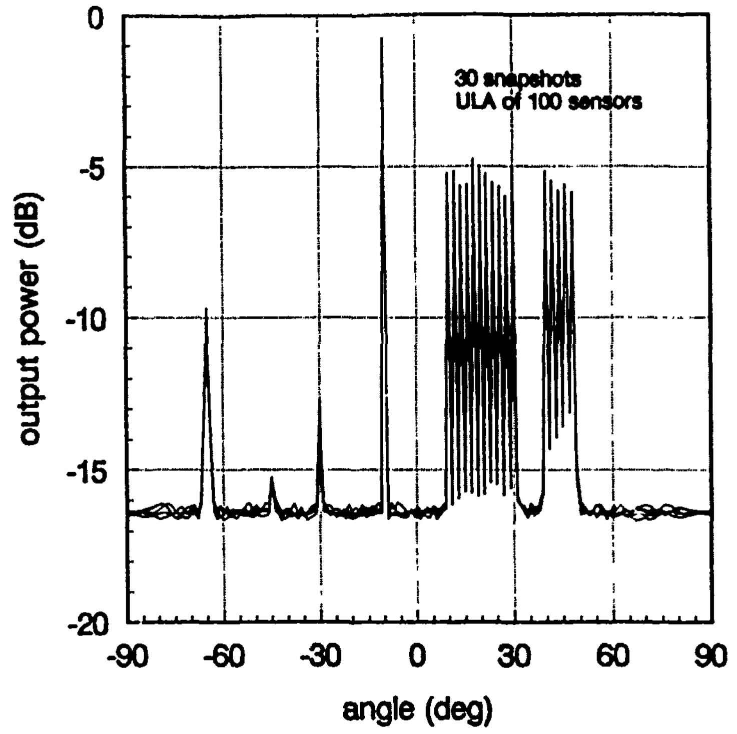

(c1) Five independent trials, each with 30 snapshots.

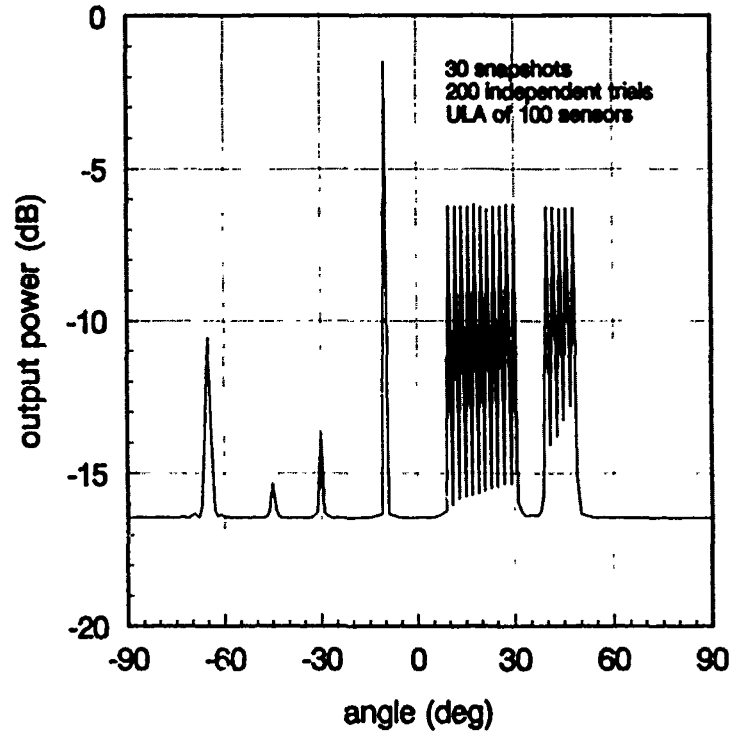

(c2) Average of 200 independent trials, each with 30 snapshots.

Figure 4 (cont.). MVDR array response with stabilization factor 0.1.

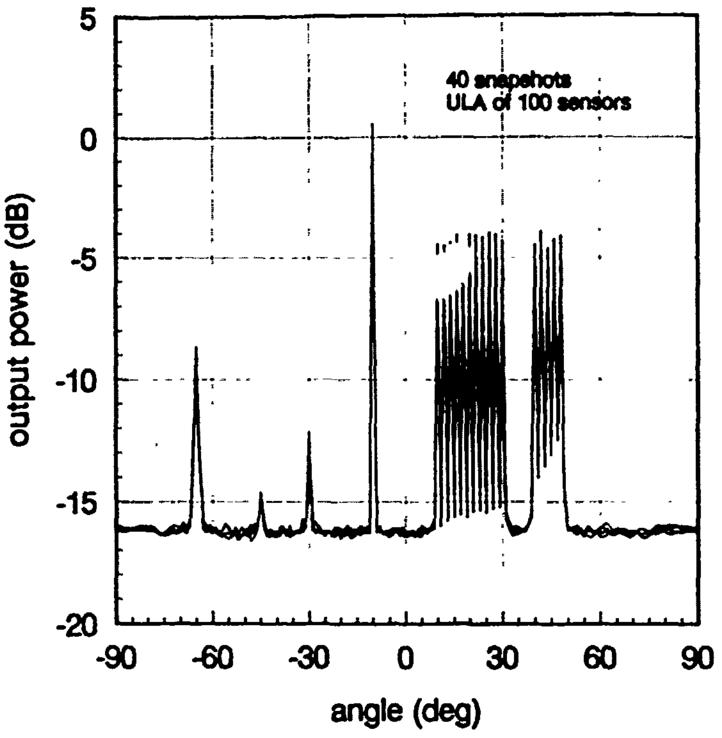

(d1) Five independent trials, each with 40 snapshots.

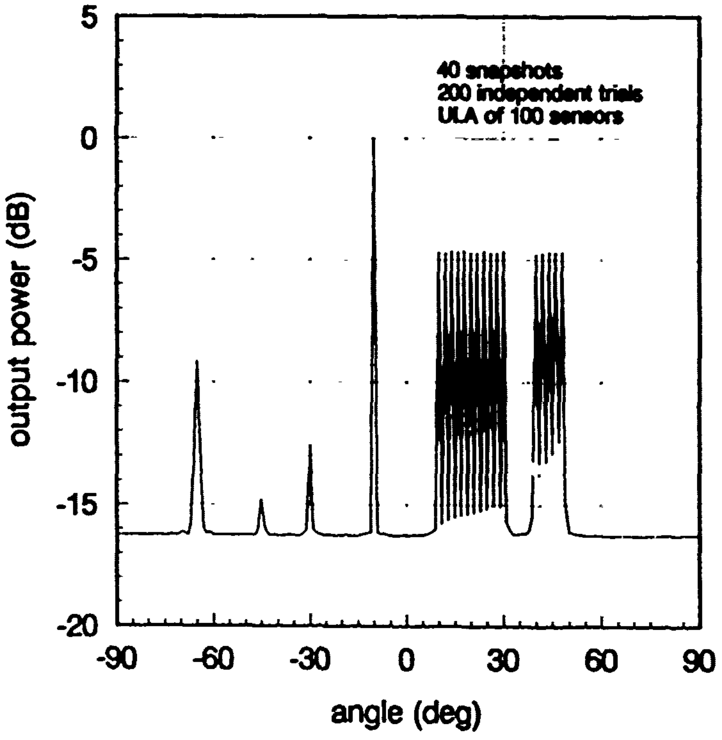

(d2) Average of 200 independent trials, each with 40 snapshots.

Figure 4 (cont.). MVDR array response with stabilization factor 0.1.

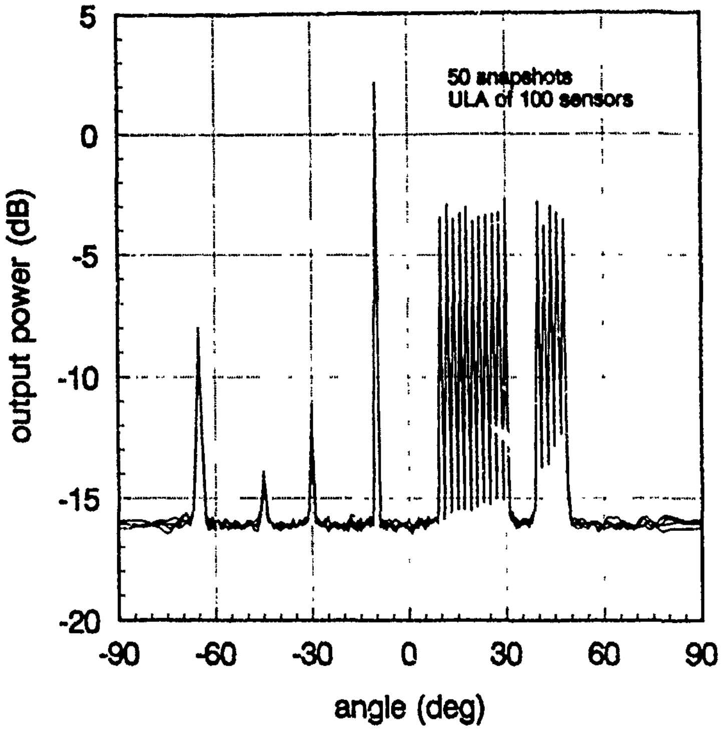

(e1) Five independent trials, each with 50 snapshots.

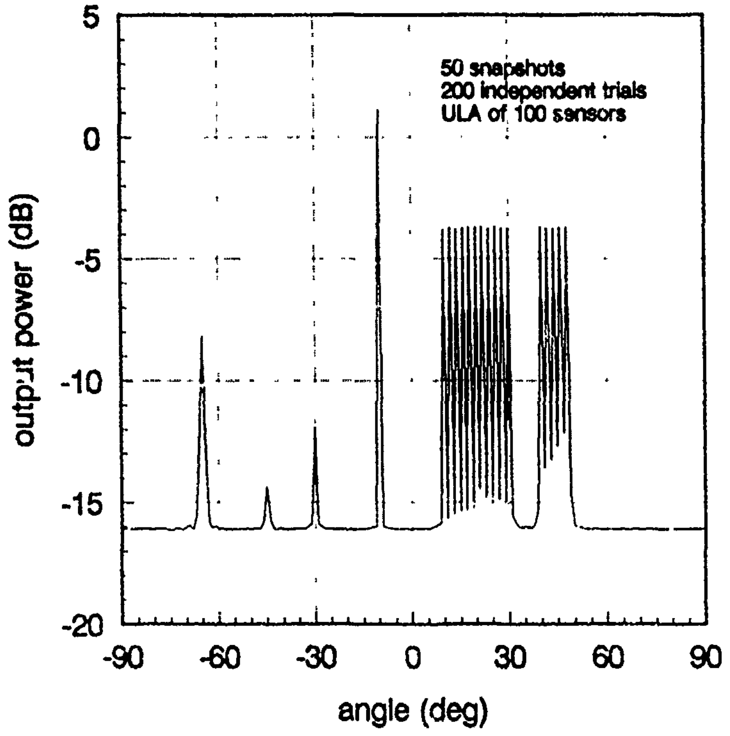

(e2) Average of 200 independent trials, each with 50 snapshots.

Figure 4 (cont.). MVDR array response with stabilization factor 0.1.

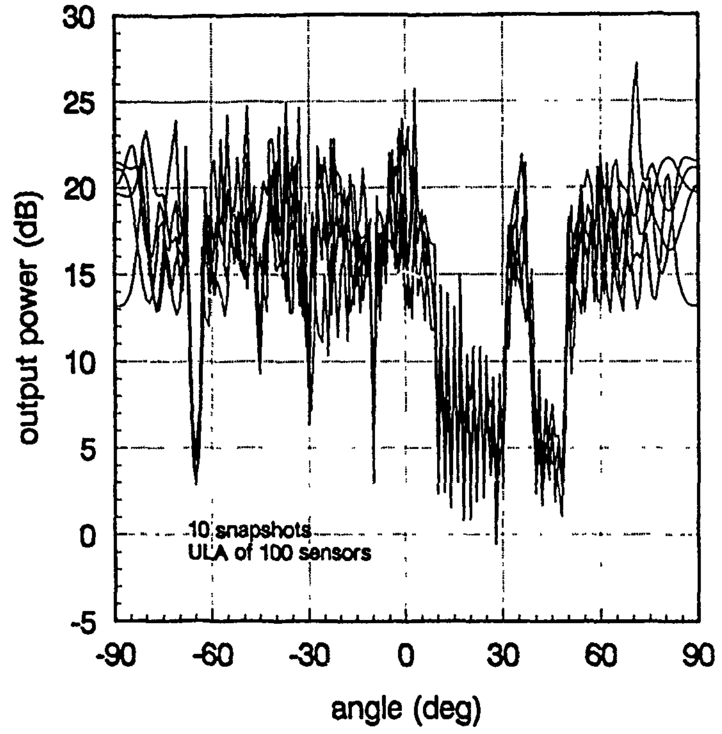

(a1) Five independent trials, each with 10 snapshots.

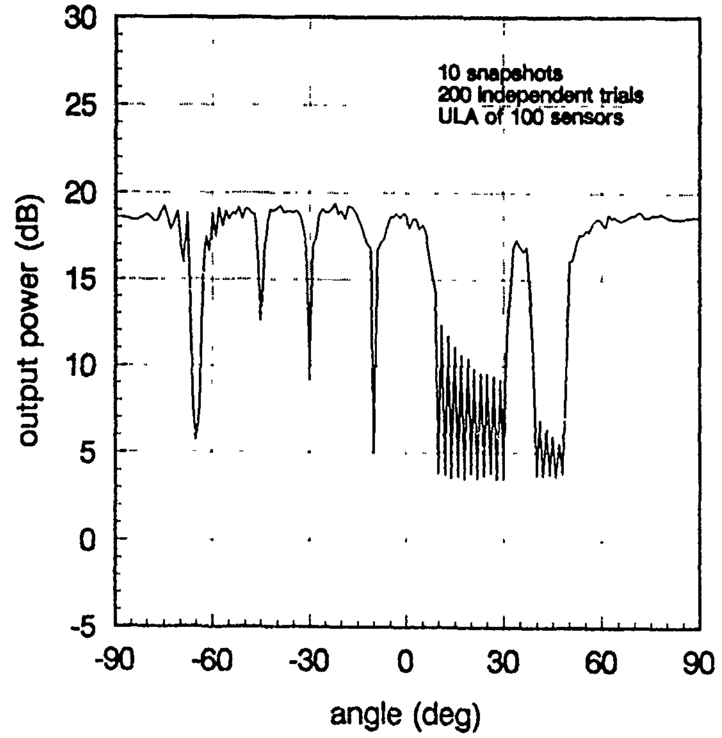

(a2) Average of 200 independent trials, each with 10 snapshots.

Figure 5. JASON array response.

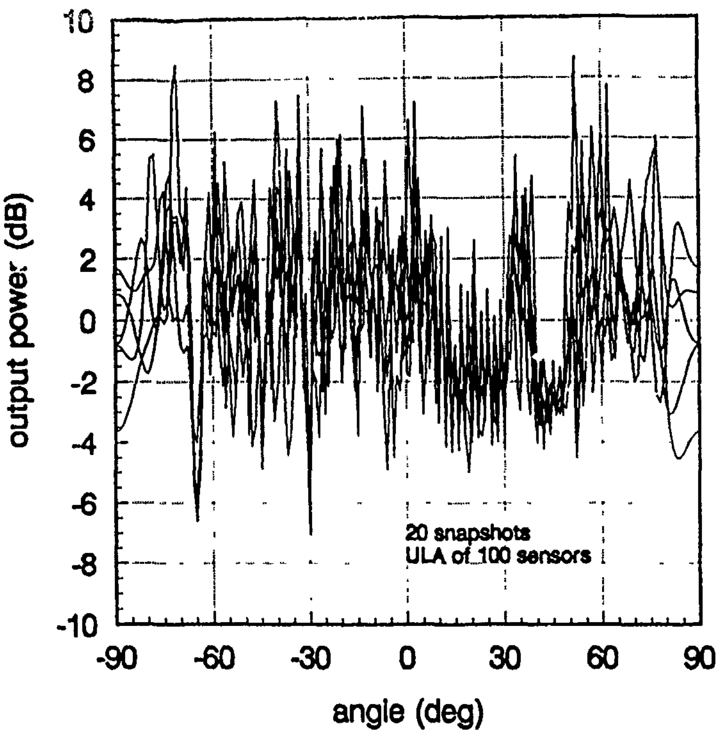

(b1) Five independent trials, each with 20 snapshots.

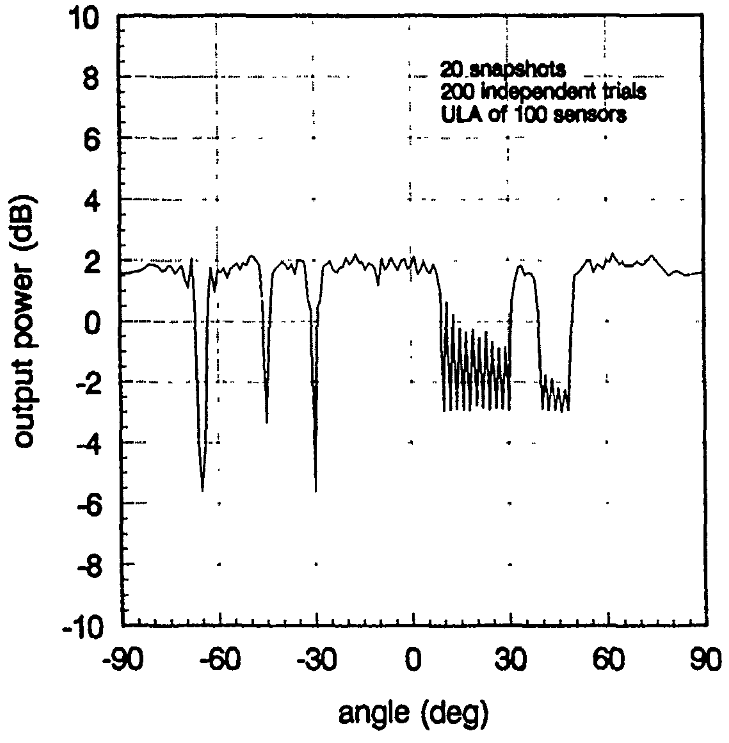

(b2) Average of 200 independent trials, each with 20 snapshots.

Figure 5 (cont.). JASON array response.

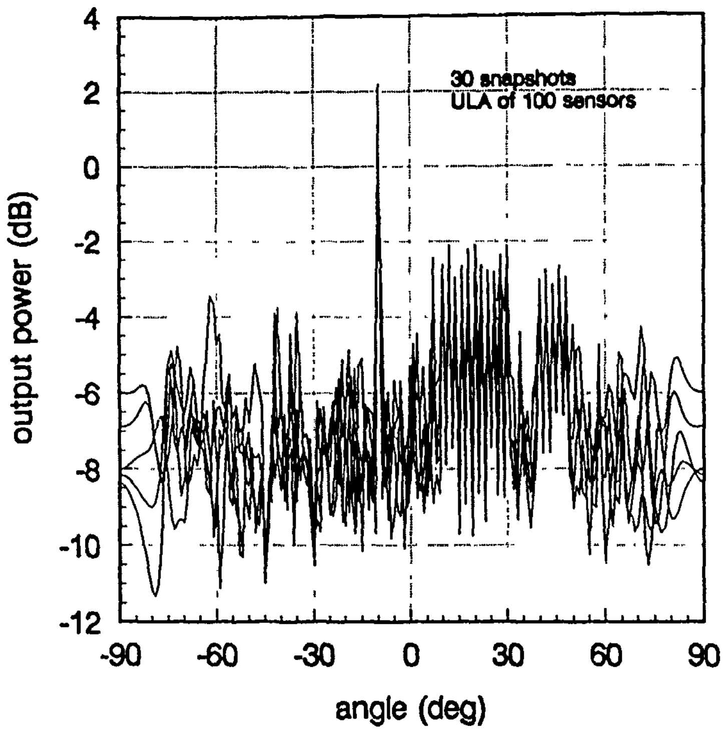

(c1) Five independent trials, each with 30 snapshots.

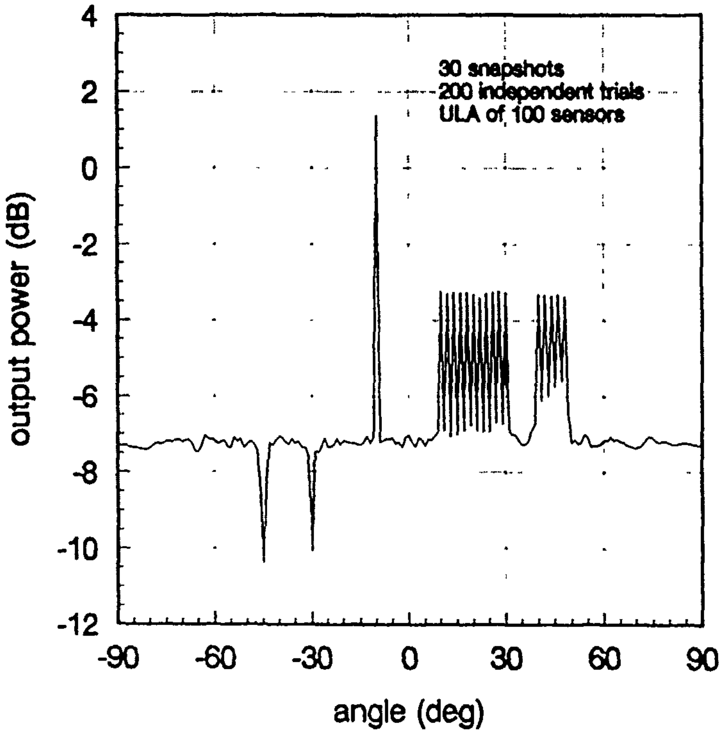

(c2) Average of 200 independent trials, each with 30 snapshots.

Figure 5 (cont.). JASON array response.

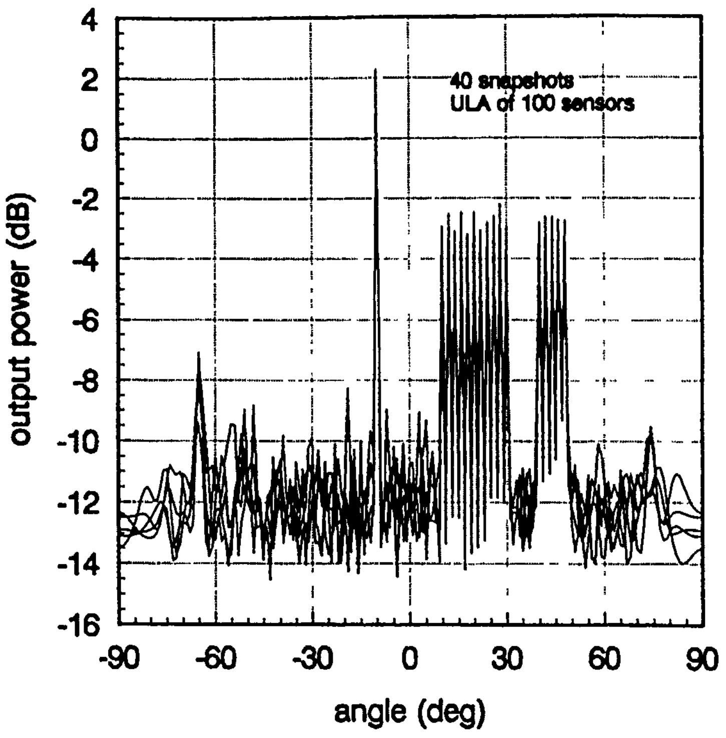

(d1) Five independent trials, each with 40 snapshots.

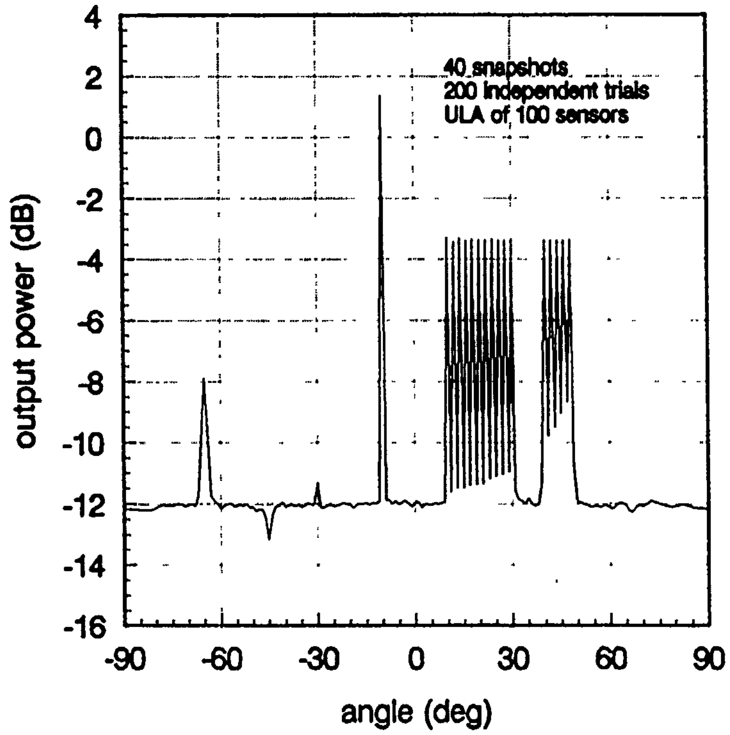

(d2) Average of 200 independent trials, each with 40 snapshots.

Figure 5 (cont.). JASON array response.

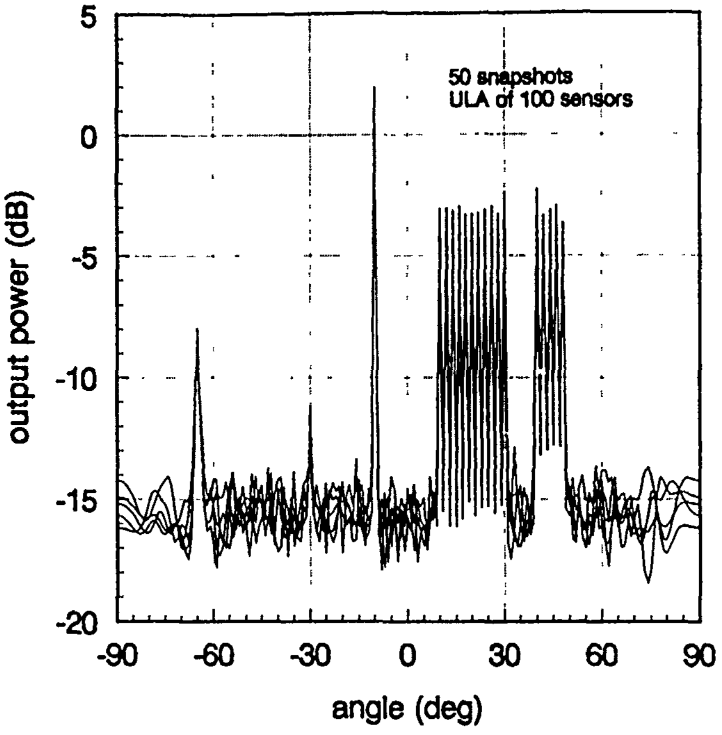

(e1) Five independent trials, each with 50 snapshots.

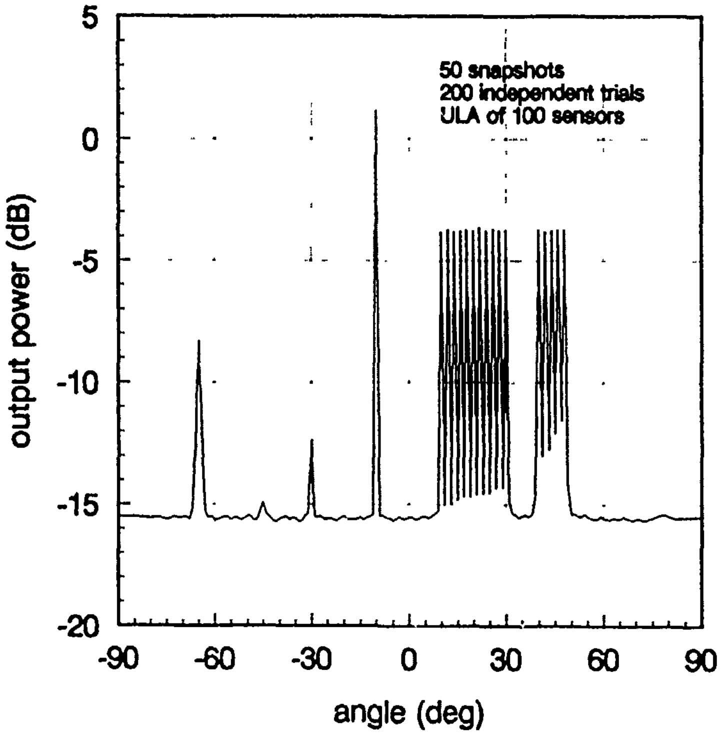

(e2) Average of 200 independent trials, each with 50 snapshots.

Figure 5 (cont.). JASON array response.

Peaks in these figures of array response should be interpreted in relative terms with respect to the corresponding background level. For example, for the 5-dB source at -10^0 with 40 snapshots, the 200-trial average output power relative to background level is about 24 dB for the conventional beamformer (figure 1(d2)), about 19.5 dB for the MVDR with stabilization factor 0.001 (figure 2(d2)), about 19 dB for the MVDR with stabilization factor 0.01 (figure 3(d2)), about 16.25 dB for the MVDR with stabilization factor 0.1 (figure 4(d2)), and about 13.5 dB for the JASON beamformer (figure 4(d2)).

The overall observation is that, for each method, the higher the number of snapshots, the lower the variability of estimate. Moreover, the higher number of snapshots also reduces the variability of background level relative to the primary peaks. For the MVDR beamformer, the higher the stabilization factor, the lower the primary peaks relative to background level, and the higher the stabilization factor, the lower the variability of background level relative to the primary peaks. Finally, among the three methods, the JASON beamformer tends to have the highest level of variability both in estimates and in background level (relative to primary peaks).

For each value of $T = 10, 20, 30, 40, 50$, the conventional beamformer tends to outperform other methods as it resolves each source with the highest peak relative to background level. This is not surprising since sources are well spaced with the smallest angular separation greater than the Rayleigh limit. Indeed, for a very large uniform array, the Rayleigh angular limit is significantly reduced, hence for all practical purposes, resolution is no longer working against the conventional beamformer as in the case of a small uniform array.

When the number of snapshots is small, we observe an inverted behavior of the JASON array response, namely, yielding a dip instead of a peak at the source's location. This inverted behavior is dependent on powers of sources. As the number of snapshots increases, sources with high SNRs begin to peak in the usual manner earlier than those with low SNRs.

To understand the inverted behavior of the JASON array response when the number of snapshots is small, let us consider the extreme case of one snapshot. For $T = 1$, then the observation matrix $\mathcal{S}$ reduces to a vector, therefore $\mathcal{S}^*\mathcal{S} = \|\mathcal{S}\|^2$ is a (positive) scalar. Consequently, the output power of the JASON beamformer corresponding to $\widehat{\mathbf{R}}$, a realization of $\mathbf{R}$, is given by

$$\mathbf{w}^*\widehat{\mathbf{R}}\mathbf{w} = \frac{(\mathcal{S}^*\mathcal{S})^2}{\gamma^*\widehat{\mathbf{R}}\gamma}. \tag{22}$$

Notice that the denominator of equation (22) is the estimated power of the conventional beamformer corresponding to $\widehat{\mathbf{R}}$. When the look-direction steering vector γ coincides with the steering vector of any source, $\gamma^*\widehat{\mathbf{R}}\gamma$ peaks and, hence, its reciprocal yields a dip at the arrival angle. Clearly the numerator $(\mathcal{S}^*\mathcal{S})^2$ of equation (22) is independent of the look-direction steering vector.

The foregoing discussion, indeed, can be recast by a short, but nonconstructive, argument: for $T = 1$,

$$\begin{aligned} \text{POWER}_{\text{JASON}} &= \mathrm{E}\left(\frac{1}{\gamma^*\mathcal{S}\,(\mathcal{S}^*\mathcal{S})^{-2}\,\mathcal{S}^*\gamma}\right) \\ &= \mathrm{E}\left(\frac{(\mathcal{S}^*\mathcal{S})^2}{\gamma^*\widehat{\mathbf{R}}\gamma}\right) \approx \frac{\mathrm{E}\left((\mathcal{S}^*\mathcal{S})^2\right)}{\mathrm{E}\left(\gamma^*\widehat{\mathbf{R}}\gamma\right)} = \frac{\mathrm{E}\left((\mathcal{S}^*\mathcal{S})^2\right)}{\text{POWER}_{\text{Con}}}. \end{aligned}$$

The inverted behavior of the JASON array response when T is small, therefore, can be explained as an extrapolation of the case of one snapshot.

5.2 Quantitative Results

To quantify output array response of each beamformer, we consider the normalized output deflection (Burdic, 1978; Krolik & Swingler, 1990) that is defined by

$$\begin{aligned} &\text{DEFLECTION}\left(\widehat{\text{POWER}}(\phi)\right) \\ &\triangleq \frac{\mathrm{E}\left(\widehat{\text{POWER}}(\phi) \mid \text{signal present}\right) - \mathrm{E}\left(\widehat{\text{POWER}}(\phi) \mid \text{signal absent}\right)}{\text{Std}\left(\widehat{\text{POWER}}(\phi) \mid \text{signal absent}\right)}, \end{aligned} \tag{23}$$

where $\widehat{\text{POWER}}(\phi)$ stands for estimated output power when steered at the angle ϕ and $\text{Std}(\square)$ denotes standard deviation of $\square$. Clearly, a high-normalized output deflection is a desirable property for detection.

To assess the relative detection performance of each beamformer when the number of snapshots is small, with interest in the detectability of a weak source in the presence of strong interferences, we compute normalized output deflection of each algorithm when the look-direction elevation angle is steered at -45^0, the direction of the weakest (-15 dB) among the twenty sources, for T running from 10 to 100 with increment equal to 5 snapshots. Each deflection estimate is obtained from 200 independent trials, using sample means of output power when steered at -45^0 either signal is present or not, and standard deviation of output power when steered at -45^0 in the absence of signal.

For real situations of multiple sources, the normalized output deflection defined as in equation (23) is difficult to estimate since one cannot recreate the same environment except for one source that now is absent. Furthermore, equation (23) is evaluated at one particular location and ignores the background that might contain spurious peaks.

An alternative to the normalized output deflection is the peak-to-background ratio, defined as

$$\frac{\text{peak output power} - \text{average background power}}{\text{standard deviation of the background power}}. \tag{24}$$

The mean background output level is usually calculated excluding a small interval around the peak (Feuillade, DelBalzo, & Rowe, 1989). Obviously, for a power detector, higher peak-to-background ratio indicates better detection.

Other things being equal, we note that, from equation (24), higher variability of background level results in lower peak-to-background ratio and, from equation (23), higher variability of estimates results in lower normalized output deflection.

For the environment of multiple sources depicted in table 1, we compute the peak-to-background ratio for the look-direction angle -45^0 as follows. The average and standard deviation of background level is calculated over the 18 grid points from -55^0 to -35^0 with 1^0 spacing, excluding output power at -46^0, -45^0 and -44^0. Peak-to-background ratio for each beamformer when steered at -45^0 is obtained as the ensemble mean of estimates from 200 independent trials. For comparison, we consider the number of snapshots from 10 to 100 with increments of 5 snapshots, that is, from $\frac{1}{10}$ of the number of sensors to the number of sensors.

Because the main lobe of the conventional beamformer is relatively wide compared to that of the MVDR and the JASON, if the interval excluded from computing the mean background output level is too small, there might be a downward bias in the resulting peak-to-background ratio for the conventional beamformer. The effect of the length of the excluded interval, however, depends on the number of elements. For the uniform linear array n elements, one measure of separation is the first-null (or standard) beamwidth, which is defined as the angular separation between the peak of the main lobe and the first null of the radiation pattern function $W(\omega) = \frac{\sin(n\omega/2)}{\sin(\omega/2)}$ where $\omega = \frac{2\pi d}{\lambda}\sin(\phi)$ with, we recall, d as the interelement spacing, λ the array wavelength, and ϕ the steering angle. Let BW denote a first-null beamwidth, then $\text{BW} = \frac{2\pi}{n}$ radians or $\frac{360}{n}$ degrees (Haykin, 1985). In our case, the excluded interval is the open interval

$$\left(-45^0 - \Delta\phi, -45^0 + \Delta\phi\right),$$

where $\Delta\phi = 2^0$. For the array of 100 equally-spaced elements with interelement spacing equal to one-half of the array wavelength, $\Delta\phi = 2^0$ amounts to $\Delta\omega = 50\sin(\pi/90)\ \text{BW} = 1.745\ \text{BW}$, and hence the immediate grid points outside the excluded interval, -47^0 and -43^0, are well separated from the main lobe.

The normalized output deflection and peak-to-background ratio of each beamformer is plotted, on linear scale and on dB scale, versus the number of snapshots. Due to the inverted behavior of the JASON array response when the number of snapshots is small relative to the number of elements, we consider absolute values of normalized output deflection and peak-to-background ratio of the JASON beamformer. This amounts to taking absolute values of the numerators of equations (23) and (24) in computing these expressions. This provision is satisfactory for detection assessment.

Overall results of normalized output deflection and peak-to-background ratio are essentially the same. The only noticeable difference between these two metrics occurs for the MVDR, as a group, when the number of snapshots is under 25. Figure 6(b) shows that the normalized deflection of the MVDR for each of the three different stabilization factors is approximately 8 dB, 4 dB, and 3 dB below the normalized deflection of the conventional beamformer for $T = 10$, 15, and 20, respectively. For these values of T, figure 7(b) indicates that the peak-to-background ratio of the conventional beamformer is less than 2 dB above that of the MVDR for each stabilization factor. This discrepancy might be attributed to the fact noted earlier that the normalized output deflection is computed when steered at a particular angle (-45^0) without taking into consideration the existence of spurious peaks in the background of the source. When T is as low as 10, 15 or 20, the relatively less variable background of the MVDR beamformer (figures 2(a1) to 2(b2), figures 3(a1) to 3(b2), and figures 4(a1) to 4(b2)), accounts for small standard deviation of background level, and thus higher peak-to-background ratio compared to the corresponding normalized output deflection.

Results in figures 6(a) and 7(a) show that, for the MVDR beamformer, there is an indication that higher stabilization factor yields higher deflection and higher peak-to-background ratio, and the effect increases as the number of snapshots approaches the number of elements. This is consistent with earlier qualitative observations that both higher number of snapshots and higher stabilization factor promote smaller standard deviation of estimate and smaller standard deviation of background level relative to primary peaks. When the number of snapshots $T \leq 50$, on the dB scale, figure 6(b) indicates that, for the MVDR beamformer with stabilization factors 0.001, 0.01, and 0.1, the differences in normalized output deflection are within 1 dB. The same observation is noted for the MVDR's peak-to-background ratios in figure 7(b) when $T \leq 50$.

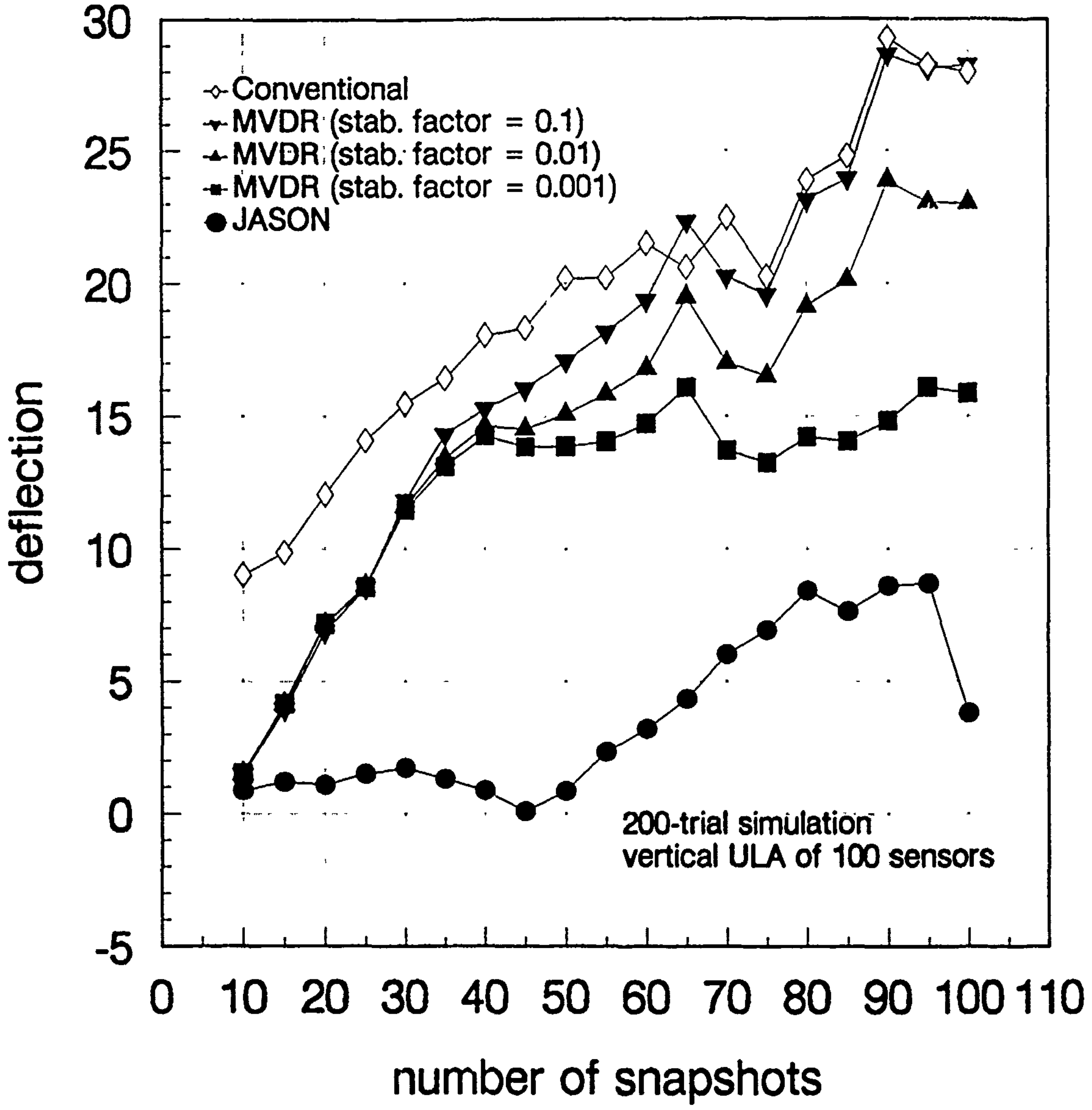

Figure 6(a). Normalized output deflection (on linear scale, with absolute value for JASON) versus number of snapshots for the source with angle-of-arrival -45^0.

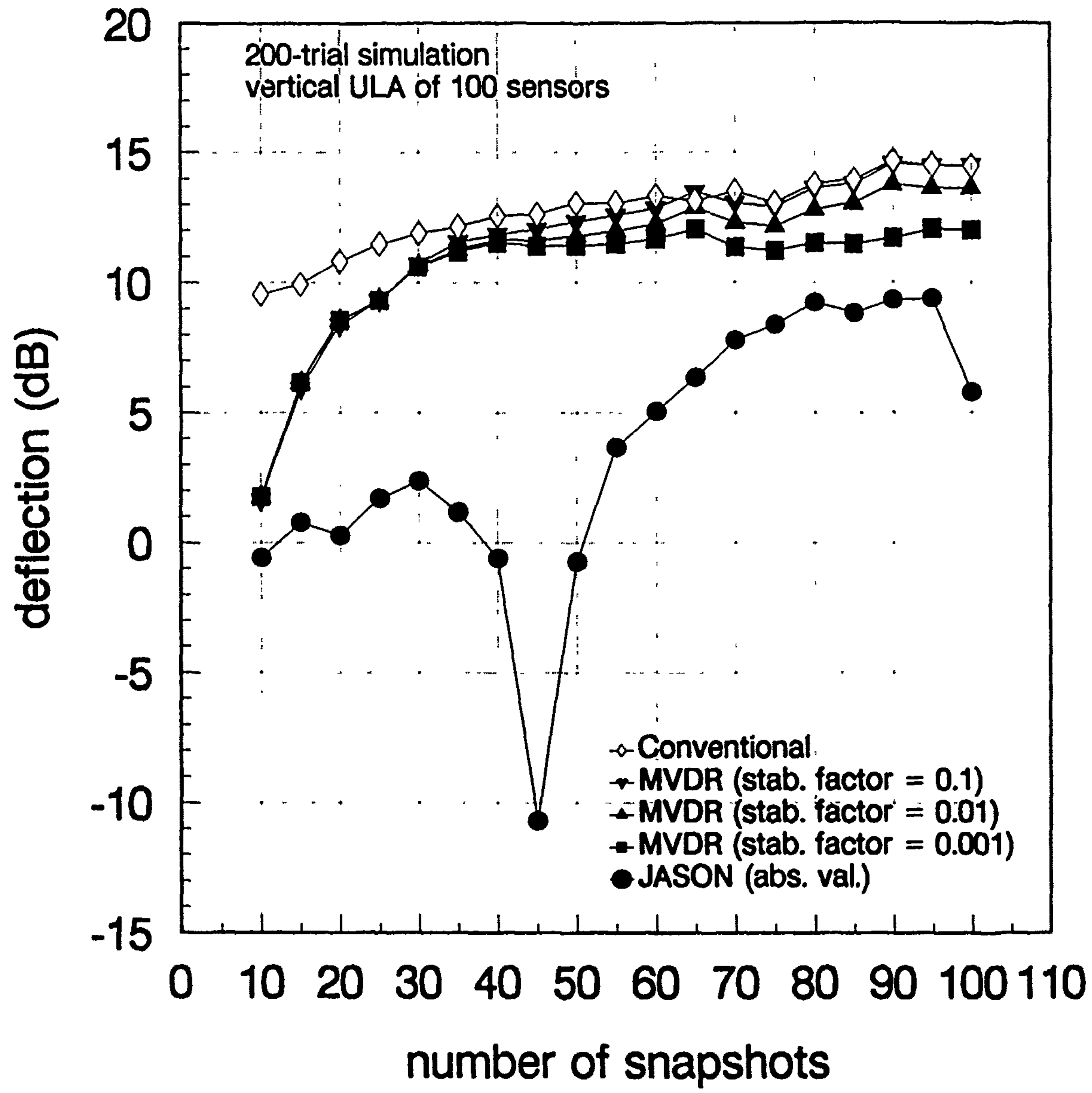

Figure 6(b). Normalized output deflection (on linear scale, with absolute value for JASON) versus number of snapshots for the source with angle-of-arrival -45^0.

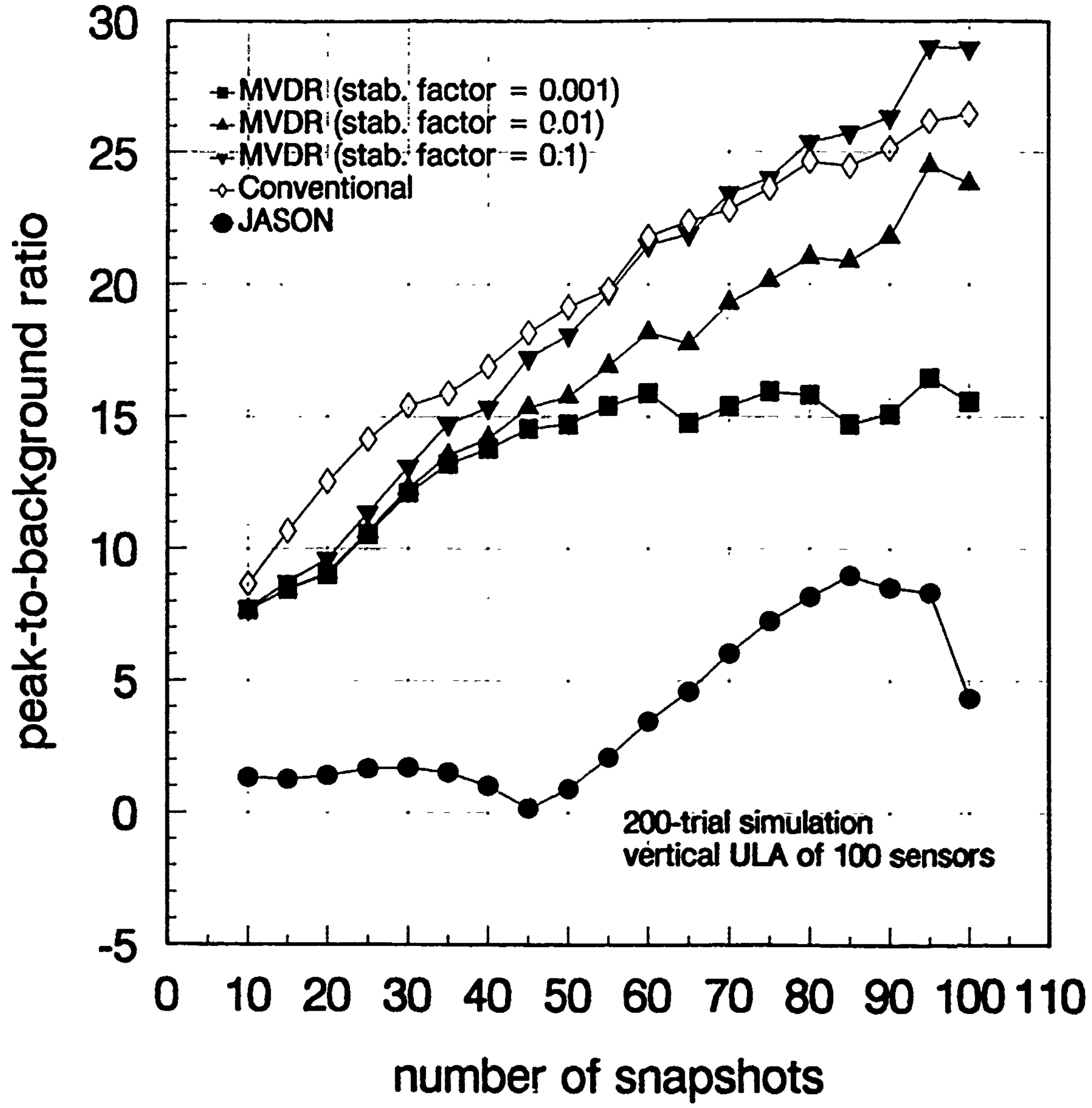

Figure 7(a). Peak-to-background ratio (on linear scale, with absolute value for JASON) versus number of snapshots for the source with angle-of-arrival -45^0.

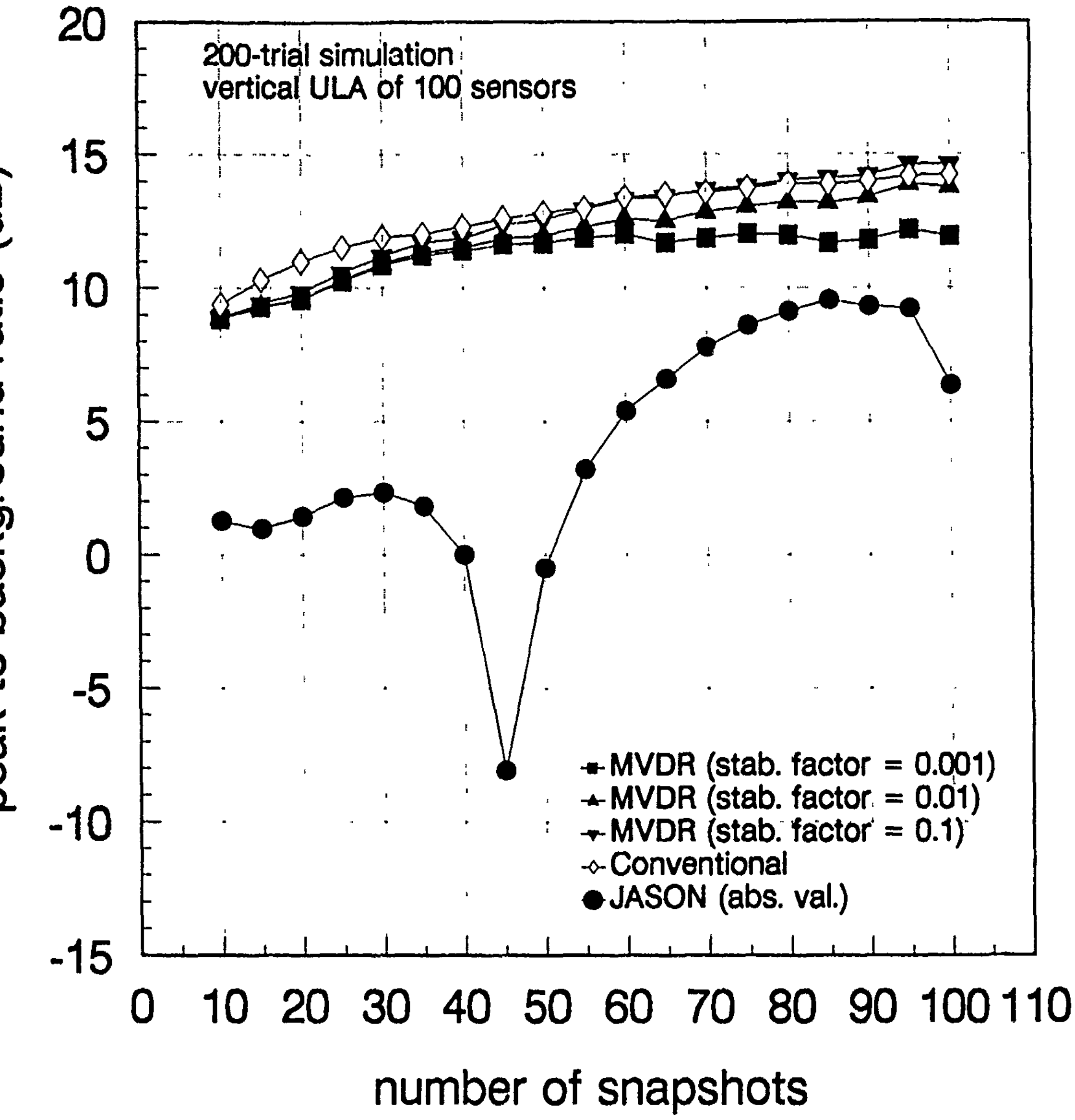

Figure 7(b). Peak-to-background ratio (on dB scale, with absolute value for JASON) versus number of snapshots for the source with angle-of-arrival -45^0.

For the JASON beamformer, when the number of snapshots is small compared to the number of sensors, all in all, the low normalized output deflection is the result of high variability of the estimate; similarly its low peak-to-background ratio is a result of high variability of background level. The dip at $T = 45$ in figure 6(b) and figure 7(b) is a superficial artifact resulting from the of taking absolute values of normalized deflection and peak-to-background ratio. Indeed, for $T \leq 40$, both normalized deflection and peak-to-background ratio are negative and relatively larger, in absolute values, than the corresponding one at $T = 45$. Therefore, taking absolute values of normalized deflection and peak-to-background ratio yields a mirror image of each when $T \leq 40$ and a dip at $T = 45$, as in figures 6(a) and 7(a); this effect is accentuated on the dB scale, as in figures 6(b) and 7(b).

6. CONCLUSION

The properties and performance of conventional, Minimum Variance Distortionless Response (MVDR), and JASON beamformers were investigated via simulation for a multiple-source environment corrupted by colored noise with special emphasis on the situation where the number of snapshots is small compared to the number of array elements. All in all, for a uniform linear array of 100 elements with interelement spacing equal to one-half of the array wavelength, when sources are well separated, the conventional beamformer tends to outperform the other two methods as it resolves each source with the highest peak relative to background level. With attention to large arrays, the choice of well separated sources in the study is justified. Indeed, for a very large uniform array, the Rayleigh angular limit is significantly reduced. Hence for all practical purposes, resolution is no longer working against the conventional beamformer as in the case of a small uniform array. The MVDR beamformer, with white-noise stabilization, displays better resolution exemplified by sharp peaks at the expense of inverting of the modified cross-spectral density matrix, a computational burden for a well-populated array. For the MVDR beamformer, we further notice that the higher the stabilization factor, the lower the variability of background level relative to the primary peaks as well as the lower the primary peaks relative to background level. The recently introduced JASON beamformer exhibits an inverted behavior, namely yielding a dip instead of a peak at source location, when the number of snapshots is small compared to the number of sensors. This inverted behavior of the JASON array response can be explained as an extrapolation of the behavior for the special case of one snapshot. Moreover, the behavior is more persistent for sources with low SNRs. As the number of snapshots increases, sources with high SNRs begin to peak in the usual manner earlier than those with low SNRs.

Quantitative results, based on normalized output deflection and peak-to background ratio, indicated better detection performance of conventional and MVDR beamform ers. When the number of snapshots is small relative to the number of array elements, the low normalized output deflection of the JASON algorithm is caused by the high variability of the estimate, and similarly its low peak-to-background ratio is a result of the high variability of background level.

Findings presented in this report were based on the simulation using an array model with relatively low-average sidelobes. Some improvements of the performance of the adaptive algorithms, especially the modified MVDR, relative to conventional beamforming might be expected for an array model with high sidelobes.

7.0 REFERENCES

[1] Burdic, W., "Detection of Narrowband Signals Using Time-Domain Adaptive Filters," *IEEE Trans. Aerosp. Electron. Syst.,* vol. 14, no. 4, pp. 578-591, 1978.

[2] Capon, J. "High Resolution Frequency-Wavenumber Spectrum Analysis," *Proc. IEEE,* vol. 57, no. 8, pp. 1408-1418, 1969.

[3] Carlson, B. D., "Covariance Matrix Estimation Errors and Diagonai Loading in Adaptive Array," *IEEE Trans. Aerosp. Electron. Syst.,* vol. 24, no. 4, pp. 397-401, 1988.

[4] Feuillade, C., D. DelBalzo, and M. Rowe, "Environmental Mismatch in Shallow-Water Matched-Field Processing: Geoacoustic Parametei Variability," *J. Acoust. Soc. Am.,* vol. 85, no. 6, pp. 2354-2363, 1989.

[5] Haykin, S., "Radar Array Processing for Angle of Arrival Estimation," in *Array Signal Processing,* ed. S. Haykin, Prentice-Hall, Englewood Cliffs, NJ, 1985.

[6] Krolik, J. and D. Swingler, "The Detection Performance of Coherent Wideband Focusing for a Spatially Resampled Array," *Proc. ICASSP-90,* Albuquerque, NM, 1990.

[7] Krolik, J. and D. Swingler, "Multiple Broad-Band Source Location Using Steered Covariance Matrices," *IEEE Trans. Acoust., Speech, Signal Processing,* vol. 37, no. 10, 1989.

[8] Melsa, J. L., and A. P. Sage, *An Introduction to Probability and Stochastic Processes,* Prentice-Hall, Englewood Cliffs, NJ, 1973.

[9] Reed, I. S., J. D. Mallett, and L. E. Brennan, "Rapid Convergence Rate in Adaptive Arrays," *IEEE Trans. Aerosp. Electron. Syst.,* vol. 10, no. 6, pp. 853-863, 1974.

[10] Rothaus, O., *Processing in Large Acoustic Arrays,* Report JSR-90-170, JASON, MITRE Corp., McLean, VA, 1991.

[11] Tran, J-M., *Approaches to the Processing of Data from Large Aperture Acoustic Vertical Line Arrays,* University of California, San Diego, Ph.D. Thesis, 1990.

APPENDIX A

MATLAB Code for Plotting Array Response

For illustration, an interactive MATLAB code for plotting array response of a uniform linear array is presented in this appendix.

The following code is runnable on 8086/8088-based computers (PC/XT) with PC-MATLAB, or on 80286-based computers (AT) with AT-MATLAB. However, these versions limit vectors to a length of 8188 elements and square matrices to order 90. It is preferable to run the code on 80386-based computers with 386-MATLAB where variables can have unlimited size, subject to only the ammount of memory installed and the amount of free hard-disk space.

Upon execution, the code will ask for inputs including the following:

> the number of sensors n,
> the number of snapshots T,
> the number of (plane wave) sources k,
> angle-of-arrival (AOA) and signal-to-noise ratio (SNR) of each source, and
> the number of independent trials.

The user is able to choose among JASON, MVDR, and conventional beamformers for plotting array response. For MVDR, the user is prompted to specify a value for stabilization factor between 0.001 and 0.1. Clearly, for $T \geq n$, a value of zero can be supplied, provided the resulting cross-spectral density matrix is not ill-conditioned.

The code then computes and plots the array response of each independent trial and the corresponding average, together on the same axes of the first plot. For JASON algorithm, due to its high variability of estimate, peaks of subsequent trials may be out of range of the first plot, especially when n is small and T is smaller than n. We did not attempt to adjust the axes to accommodate all trials.

```
%    RESPONSE.M
%    Cam Tran
%    Monday June 10, 1991
%
%    INTERACTIVE CODE FOR PLOTTING ARRAY RESPONSE OF CHOICE AMONG
%    * JASON
%    * MVDR (with white-noise stabilization)
%    * CONVENTIONAL
%
%    ARRAY: ULA WITH INTERELEMENT SPACING = 1/2 WAVELENGTH
%    SOURCES: PLANE WAVES
%    ARRAY RESPONSES OF A FINITE NUMBER OF TRIALS (USER-SPECIFIED) ARE PLOTTED
%    A PLOT OF THE AVERAGE ARRAY RESPONSE IS ALSO INCLUDED.
%
clear, clc, clg
n = input('ENTER number of sensors: ');
T = input('ENTER number of snapshots: ');
k = input('ENTER number of sources: ');
rand('normal')
for sindex = 1:1:k
    phi(sindex) = input(['ENTER AOA of signal vector #', num2str(sindex), ' (-90 deg to 90 deg): ']);
    SNR(sindex) = input(['ENTER SNR of signal #', num2str(sindex), ' (in dB): ']);
    dSNR(sindex) = 10^(0.1*SNR(sindex));
end
%
test = input('ENTER 0 for JASON, 1 for MVDR, 2 for Conventional: ');
if test == 1
    stafact = input('ENTER stability factor (between 0.001 to 0.1): ');
end
%
numrun = input('ENTER number of independent trials: ');
```

```
%
%   Columns of the matrix below are steering vectors of k sources
%
index=1:1:n;
alpha = exp( -i*( ( ((n-1)/2) - index' + 1 ) * pi * sin(phi*pi/180) ) );
%
numpts = 181;      %   number of look directions
%
%   SIMULATION LOOP
%
counter = numrun;
%
%   Initialize the matrix sumtemp that will be used to accumulate
%   output powers from numrun independent trials.
%
sumtemp = zeros(1,numpts);
%
while counter > 0
    %
    %   Normalize the random matrix Ntemp := rand(n,T) + i*rand(n,T)
    %   to obtain scriptN with and (1 / Tn ) * trace( scriptN * scriptN' ) = 1.
    %
    Ntemp = rand(n,T) + i*rand(n,T);
    scriptN = ( sqrt(T*n) / norm(Ntemp,'fro') ) * Ntemp;
    %
    %   Compute simulated observation matrix scriptS := [ X(t) | X(t+1) | ... | X(t+T-1)]
    %   = scriptN + alpha(1)*(scriptP(1))' + ... + alpha(k)*(scriptP(k))'
    %
    scriptS = scriptN;      %   initialize scriptS
    for sindex = 1:1:k
        %   The Ptemp are complex vectors such that the real part and the complex part of
        %   each of their entries are normally distributed with means 0.0 and variances 1.0
    %
    Ptemp = rand(T,1) + i*rand(T,1);
    %
    %   Normalizing Ptemp to obtain scriptP such that (scriptP'*scriptP)/T = dSNR(sindex)
    %
    scriptP = sqrt( T*dSNR(sindex) / (Ptemp'*Ptemp) ) * Ptemp;
    %
    scriptS = scriptS + alpha(:,sindex) * scriptP';      %    accumulate scriptS
end
%
if test == 1
%   This part is for MVDR only.
    %   Adding to the estimated CSDM = (1/T)*scriptS*scriptS'
    %   the matrix epsilon*Identity where epsilon = stafact*trace(CSDM)/n
    %   with stabilization factor stafact usually chosen between 0.001 and 0.1
%
    Mtemp = scriptS*scriptS';      %    T * CSDM
    Tepsilon = stafact * sum(diag(Mtemp)) / n;      %    T * epsilon
    Mtemp = ( Mtemp + Tepsilon*eye(n) ) / T;      %    CSDM after diagonal loading
end
%
if test == 0
    jpower = zeros(1,numpts);
    jMtemp = inv(scriptS' * scriptS * scriptS' * scriptS);
    jMtemp = scriptS * jMtemp * scriptS';
elseif test == 1
    mpower = zeros(1,numpts);
    mMtemp = inv(Mtemp);
else
    cpower = zeros(1,numpts);
    cMtemp = scriptS * scriptS';
end
```

```
%
gindex=1:1:numpts;
angle = -90 + 1*(gindex -1);
omega = pi * sin(angle*pi/180);
%
for gindex=1:1:numpts
    %
    %   Look-direction steering vectors
    %
    index=1:1:n;
    gamma = exp( -i*( ( ((n-1)/2) - index + 1 ) * omega(gindex) ) );
    gamma = conj(gamma');       %   columns of gamma are look-direction steering vectors
    %
    if test == 2
        cpower(gindex) = ( gamma' * cMtemp * gamma ) / T;       %  conventional output power
    elseif test == 0
        jpower(gindex) = 1 / ( T * gamma' * jMtemp * gamma );       %   JASON output power
    else
        mpower(gindex) = 1 / ( gamma' * mMtemp * gamma );       % MVDR output power
    end
    %
end       %   of "for gindex=1:1:numpts"
%
%   Accumulate output powers
%
if test == 0
    sumtemp = sumtemp + jpower;
elseif test == 1
    sumtemp = sumtemp + mpower;
else
    sumtemp = sumtemp + cpower;
end
```

```
    %
    %   Plotting array response
    %
    if test == 2
        plot(angle, 10*log10(cpower),'-')
        title('Conventional Array Reponse')
    elseif test == 0
        plot(angle, 10*log10(jpower),'-')
        title('JASON Array Reponse')
    else
        plot(angle, 10*log10(mpower),'-')
        title(['MVDR Array Reponse (stabilization factor = ', num2str(stafact), ')'])
    end
    %
    grid
    xlabel('angle (deg)')
    ylabel('output power (dB)')
    %
    if numrun > 1
        hold on
    end
    %
    counter = counter - 1;
    %
end     %   of "while counter > 0"
%
%   Compute the average power
avgpower = sumtemp / numrun;
%   Plot average output power from the numrun independent trials
plot(angle, 10*log10(avgpower),'g')
hold off
%   END OF CODE
```

REPORT DOCUMENTATION PAGE	*Form Approved OMB No. 0704-0188*

1. AGENCY USE ONLY *(Leave blank)*	2. REPORT DATE October 1991	3 REPORT TYPE AND DATES COVERED Final
4 TITLE AND SUBTITLE BEAMFORMING WITH A LIMITED NUMBER OF SNAPSHOTS		5 FUNDING NUMBERS PE: 0602314N WU: DN308291
6 AUTHOR(S) C. V. Tran		
7. PERFORMING ORGANIZATION NAME(S) AND ADDRESS(ES) Naval Ocean Systems Center San Diego, CA 92152–5000		8. PERFORMING ORGANIZATION REPORT NUMBER TD 2226
9 SPONSORING/MONITORING AGENCY NAME(S) AND ADDRESS(ES) Office of Chief of Naval Research Arlington, VA 22217		10 SPONSORING/MONITORING AGENCY REPORT NUMBER
11. SUPPLEMENTARY NOTES		
12a. DISTRIBUTION/AVAILABILITY STATEMENT Approved for public release; distribution is unlimited.		12b. DISTRIBUTION CODE

13 ABSTRACT *(Maximum 200 words)*

This report investigates the properties and the performance of the conventional (or Bartlett), the MVDR, and the JASON beamformers when the number of snapshots is small compared to the number of array elements.

14. SUBJECT TERMS conventional beamformer JASON beamformer MVDR beamformer			15 NUMBER OF PAGES 70
			16 PRICE CODE
17. SECURITY CLASSIFICATION OF REPORT UNCLASSIFIED	18 SECURITY CLASSIFICATION OF THIS PAGE UNCLASSIFIED	19 SECURITY CLASSIFICATION OF ABSTRACT UNCLASSIFIED	20 LIMITATION OF ABSTRACT SAME AS REPORT

UNCLASSIFIED

21a. NAME OF RESPONSIBLE INDIVIDUAL	21b TELEPHONE *(Include Area Code)*	21c. OFFICE SYMBOL
C. V. Tran	(619) 553-2524	

NSN 7540-01-280-5500

Standard form 298

UNCLASSIFIED

INITIAL DISTRIBUTION

Code 0012	Patent Counsel	(1)
Code 0144	R. November	(1)
Code 7304	G. Mohnkern	(1)
Code 76	F. M. Tirpak	(1)
Code 761	G. W. Byram	(1)
Code 761	C. V. Tran	(7)
Code 952B	J. Puleo	(1)
Code 961	Archive/Stock	(6)
Code 964B	Library	(3)

Defense Technical Information Center
Alexandria, VA 22304-6145 (4)

NOSC Washington Liaison Office
Arlington, VA 22217

Center for Naval Analyses
Alexandria, VA 22302-0268

Navy Acquisition, Research & Development
Information Center (NARDIC)
Alexandria, VA 22333

Navy Acquisition, Research & Development
Information Center (NARDIC)
Pasadena, CA 91106-3955

Naval Underwater Systems Center
New London, CT 06320-5594

Naval Research Laboratory
Washington, DC 20375-5000

Scripps Institution of Oceanography
San Diego, CA 92152-6400 (2)

Yale University
Department of Electrical Engineering
New Haven, CT 06520

JASON, MITRE Corporation
McLean, VA 22102-3481

SUPPLEMENTARY

INFORMATION

DEPARTMENT OF THE NAVY
NAVAL COMMAND CONTROL AND OCEAN SURVEILLANCE CENTER
RESEARCH DEVELOPMENT TEST AND EVALUATION DIVISION
SAN DIEGO, CALIFORNIA 92152-5000

IN REPLY REFER TO:

ERRATA AD-A244346

5000
Ser 761/10
28 Feb 92

From: Commanding Officer, Naval Command, Control and Ocean Surveillance Center RDT&E Division

Subj: ADDENDUM TO NOSC TECHNICAL DOCUMENT 2226

Ref: (a) NOSC Technical Document 2226 of Oct 1991

Encl: (1) Ltr of 19 Feb 92 from Professor Oscar S. Rothaus of MITRE Corporation

1. Enclosure (1) is a letter from Professor Oscar S. Rothaus and is being distributed to the recipients of Ref (a) per his request. He has advanced an alternate explanation for the apparent performance anomalies of the JASON beamforming algorithm and suggested modifications and further simulation.

2. Our funding in this area has ended so we are not able to further explore Professor Rothaus' suggestions.

3. We hope that distribution of the letter will provide additional insight and stimulate further work in this interesting area.

4. If you have any questions, please feel free to contact George Byram at 619-553-2543. The FAX number is 619-553-2537.

George Byram
GEORGE BYRAM
By direction

Distribution:
DTIC
NCCOSCLIAOFF
CNA
NARDIC, Alexandria
NARDIC, Pasadena
NUSC
NRL
Scripps Institute of Oceanography
Yale University
MITRE Corporation, McLean, VA

Copy to:
0012
0144 (November)
7304 (Mohnkern)
76
761 (Byram, Tran)
952B (Puleo)
961 (Archive, Stock)
964B

Writer: G. Byram, x32543
Typist: S. Gossom, 28 Feb 92

JASON

MITRE

February 19, 1992

Dr. C. V. Tran
Naval Oceans Systems Center
Code 761 (Topside)
San Diego, CA 92152-5000

Dear Dr. Tran:

With your report, computer runs, and calculations all before me in NOSC Technical Document 2226, October 1991 on "Beamforming with a Limited Number of Snapshots," I can now clearly see why the JASON beamforming algorithm investigated in your report appears to perform so poorly when compared to conventional Bartlett and also MVDR with diagonal loading.

I believe the distortion arises from a misinterpretation of the JASON algorithm, and from your choice thereby of the measure of its effectiveness. I will explain in more detail momentarily.

I must also admit to being disappointed at seeing nothing in your report about the JASON work on projected length of steering vectors into signal subspace – you made some computer runs on these questions which showed very interesting behavior. These considerations did form an integral, though incomplete, part of the JASON algorithm, and might have stimulated further research. While I personally intend none further, I fear your report in its present form will end all research in these directions.

Let me begin with the misinterpretation. You reinterpreted the JASON algorithm as just another beamforming procedure, and appraised its performance in a fairly standard fashion. You began by noting, as does one of the key arguments in the JASON report, that if the look direction steering vector γ is in the range space of the covariance matrix R, (and this is the typical state of affairs when signal is present in direction γ), then the weight vector for MVDR beamforming can also be assumed to lie in the range space. Hence one can minimize w^*Rw subject to $w^*\gamma = 1$, with the additional stipulation that w is in the range space of R. This leads, as the JASON report happily notes, to inverting a substantially smaller matrix than the conventional diagonally loaded MVDR. But now you go on to use the actual constrained minimum of w^*Rw with the additional stipulation above as the array response for any look direction of JASON beamforming. No such suggestion or claim is made in the JASON report.

With this measure of array response selected, the JASON algorithm shows a bizarre inverted behavior, particularly for a small number of snapshots. While you explained this behavior in your report, I believe I have a more revealing explanation.

One must ask, how does your choice of array response behave when the look direction steering vector is not in the range space of R, the state of affairs which strongly suggests no signal is present in that direction. Well now, a very simple calculation shows that the response scales like the reciprocal of the squared length of the projection of the steering vector into the range space.

For the simulations you have chosen, with a uniform linear array, the set of discrete look direction steering vectors are almost perpendicular to each other. The direction perpendicular to the signal-present directions are thus only feebly present in the signal subspace matrix, or equally in the covariance matrix, and so the scaling factor is large in the no-signal present directions. As the number of snapshots increases, noise diffuses into all the look directions, and the distortion is reduced.

(I would not expect any kind of beamforming with geometrically dispersed sensors to work very well if the number of snapshots is much less than twice the number of "interesting" signals present. In your simulations, you are effectively getting super-resolution for Bartlett and MVDR because the steering vectors are almost perpendicular to each other.)

A more reasonable measure, then, of the JASON array response would simply be to remove the scaling factor. In the notation of your report this amounts simply to multiplying your array response measure for look direction γ by the factor:

$$\frac{\gamma^*S(S^*S)^{-1}S^*\gamma}{\gamma^*\gamma}.$$

I feel certain that the thus modified JASON array response will be quite a bit more normal in appearance. Yet I do not like this procedure still, because it is ad-hoc. The whole point of the JASON algorithm was to devise an objective statistical methodology for handling beamforming with a limited number of snapshots. The test we derived has a measure of detect which scales inversely with the length (not the squared length) of the projection of steering vector into signal subspace, and so will not misbehave quite as badly as your array response measure. But as your know, we were still very much concerned (with good reason) with the large variance of the detect, and were trying to bring, objectively, the length of the projection of the steering vector into the statistical picture. We had one suggestion for doing so, which is far from being the end of the matter, and it is here that more research needs to be done.

There is another approach to your measure of JASON array response, which leads to conclusions similar to those I have outlined above. If one knows that γ is in the range space of R, then as already noted, the minimum of w^*Rw subject to $w^*\gamma = 1$ may be sought with w in the range space of R. But suppose that the look direction is not in the range space. Then it is easy to see that the constrained minimum above is simply zero. So one might also have set the JASON array response to zero in these directions. But we have only a discrete imperfect set of look directions, and a noisy estimate of R, so it is natural to shade off all responses according to the length of the projected vectors in range space, perhaps in a manner similar to that described earlier.

I hope you will be able to perform some additional computations for the simulations described in your report, which you will circulate in a supplemental report, showing more accurately the true potential of the JASON algorithm, and which may additionally stimulate further research. I will, of course, be happy to discuss any details on further simulations with you.

I was very pleased when NOSC decided some time back to explore the JASON algorithm, and I am grateful for all the work you nave carried out to date. Perhaps I should have paid closer attention along the way, but as you can see now, I am concerned that the current report create a balanced, accurate, and forward looking description of the JASON (and JASON-like) algorithm. To this end, I believe it vital that further details be circulated.

Accordingly, if you will not be able to supplement your original report, I am going to ask you to distribute a copy of this letter to all the recipients of the original.

Very truly yours,

[illegible]

Oscar S. Rothaus

cc: Curtis G. Callan
Gerald L. Mohnkern

JSC-92-0201